**FULL TITLE:** The orphan nuclear receptor Nr2f6 impairs skeletal muscle oxidative capacity and regulates muscle mass in mice.

**SHORT TITLE:** Nr2f6 regulates muscle biology

**AUTHORS:**

Dimitrius Santiago Passos Simões Fróes Guimarães[1,2,*]

Ninon Melany Flores Barrios[1]

André Gustavo de Oliveira[1]

David Rizo-Roca[2]

Maxence Jollet[3]

Jonathon A.B. Smith[2]

Thiago Reis Araujo[1]

Marcos Vinicius da Cruz[1]

Emilio Marconato Junior[1]

Sandro Massao Hirabara[4]

André Schwambach Vieira[1]

Anna Krook[2]

Juleen R. Zierath[2,3]

Leonardo dos Reis Silveira[1]

**AFFILIATIONS:**

[1]Department of Structural and Functional Biology, University of Campinas, Campinas, Brazil

[2]Department of Physiology and Pharmacology, Karolinska Institutet, Stockholm, Sweden

[3]Department of Molecular Medicine and Surgery, Karolinska Institutet, Stockholm, Sweden

[4]Interdisciplinary Post-Graduate Program in Health Sciences, Cruzeiro do Sul University, São Paulo, Brazil

***Correspondence**

Dimitrius Santiago P.S.F. Guimarães

Centro de Pesquisa em Obesidade e Comorbidades

Universidade Estadual de Campinas - Instituto de Biologia

Rua Carl Von Linnaeus - Bloco Z

CEP 13083-862

Campinas - SP

Brazil

F: +55 (19) 3521-6191.

E-mail: dimitrius.guimaraes@ki.se; d211529@unicamp.br

**ABSTRACT**

The maintenance of skeletal muscle plasticity upon changes in the environment, nutrient supply, and exercise depends on regulatory mechanisms that couple structural and metabolic adaptations. However, the transcriptional control of both processes by nuclear receptors (NR) remains underexplored. Nr2f6 is an orphan NR and a key regulator of metabolism and differentiation. Nonetheless, its role in muscle biology remains elusive. Here, we report, for the first time, the effects of Nr2f6 modulation in skeletal muscle *in vivo* and *in vitro*. Depletion of Nr2f6 increased myocyte's oxidative capacity and sharply attenuated lipid-induced cell death, which was associated with direct derepression of uncoupling protein 3 and PGC-1$\alpha$ promoters' transactivation. Conversely, Nr2f6 overexpression in the *tibialis anterior* induced atrophy and hypoplasia, accompanied by impairment of force production and the establishment of a molecular signature of inflammation, and a decrease in genes involved in oxidative metabolism and contraction. Additionally, global transcriptomics showed that Nr2f6 upregulated core components of the cell division machinery and repressed myogenesis genes, thus decoupling myoblast proliferation from differentiation. Collectively, our findings define a novel role for Nr2f6 as a molecular transducer maintaining the balance between skeletal muscle contractile function and oxidative capacity, with implications for metabolic diseases and myopathies treatment.

**KEYWORDS:** muscle atrophy; Nr2f6; skeletal muscle; transcription; energy metabolism; nuclear receptor;

## INTRODUCTION

Muscle contraction is a highly coordinated process initiated by the transmission of the action potential from the afferent neurons to the muscle. Subsequent depolarization of the muscle fiber triggers an action potential that propagates along the sarcolemma, stimulating the release of calcium ions from the sarcoplasmic reticulum, and ultimately promoting myosin-actin cross-bridge cycling and force production. This process requires an accessory metabolic machinery to generate the energy needed to support contraction, and disruption in either muscle structure or metabolism leads to functional defects, such as in Duchenne syndrome[1], [2], sarcopenia[3], and cachexia[4]. Dynamic crosstalk between energetic status, muscle development, mechanical stress, and transcriptional changes is crucial to maintain muscle function. In this context, the nuclear receptor family of transcription factors (NR) is of particular interest since they are regulated by small molecules, such as metabolites and hormones[5]. Although the transcriptional landscape for metabolic-functional signaling has been extensively studied in pathological and physiological conditions, a broader role of some NRs has only recently been recognized, and thus, the role of many members remains elusive[6].

The NRs have a modular architecture that contains a ligand-binding domain (LBD) and a zinc-finger DNA binding domain (DBD), and can be further grouped in endogenous, orphan, or adopted NRs according to the presence of an endogenous ligand, the absence of a known ligand or if a new ligand for a given NR was just identified, respectively[7]. The classical mechanistic model proposes that a small molecule binds to the LBD, changing its conformation to one of higher affinity for a transcriptional co-regulator[8], such as PGC-1α, which in turn can mediate transcriptional modulation through the recruitment of histone acetylases, the mediator complex, and basal transcriptional apparatus.

The orphan nuclear receptor Nr2f6 (also named Ear2 or COUP-TFIII) has been characterized in a broad range of tissues, such as adipose, thyroid, liver, brain, and the immune system, where it plays different and even antagonistic roles[9]. Nr2f6 can impair adipocyte differentiation, increase cancer cell proliferation, induce both resistance and susceptibility to antitumor drugs, and promote the development

of fatty liver disease[10]. In ovarian cancer cells, Nr2f6 binds to the histone acetylase P300 at the Notch3 promoter, increasing histone H3 K9 and K27 acetylation to activate transcription, increasing cell proliferation and chemoresistance[11]. So far, the most extensively defined role of Nr2f6 is in the immune system, in which it directly and strongly suppresses interleukins 17, 21, 2 and interferon γ transcription by interacting with the NFAT/AP-1 complex at the promoters of these genes[12], [13]. Curiously, Nr2f6 has been reported both as a transcriptional repressor and activator, but the context that defines its activity state is unknown. Recently, Nr2f6 was classified as a stripe transcription factor[14], i.e. it can bind to low-complexity motifs together with other transcription factors in a broad range of promoters, regulating chromatin accessibility. This indicates that the function of Nr2f6 in diverse environments is influenced not only by its DNA occupancy but also by the presence and activity of other transcription factors. Whether the current understanding of the role of Nr2f6's can be applied to other tissues, such as skeletal muscle is unknown. Therefore, we sought to characterize the molecular mechanisms and functional roles of Nr2f6 in skeletal muscle biology both in vitro and in vivo. We discovered that Nr2f6 overexpression in skeletal muscle disrupts oxidative metabolism by directly repressing PGC-1α and the uncoupling protein 3 (UCP3) gene expression, which impairs mitochondrial function. Moreover, Nr2f6 induces core genes of cell cycle progression and in skeletal muscle activates immune cells, increasing inflammation, reducing mass, changing fiber type, and reducing force production, collectively causing a sarcopenic-like state.

## RESULTS

### Nr2f6 regulates muscle cell metabolism and differentiation.

Genetic manipulations of Nr2f6 at the whole-body level and *in vitro* have been conducted[10], [11], [23], [24], but the role of this NR in muscle models is underexplored. We used siRNA-mediated depletion of Nr2f6 in C2C12 myocytes to verify the outcomes on the transcriptomic landscape (Supplementary Figure 1A). The 1849 differentially regulated genes, 920 upregulated and 939 downregulated, could be grouped into five main classes, with increased expression of genes related to

muscle differentiation, contraction, and metabolism and decreased expression of genes with roles in cell cycle and DNA packaging (Figure 1A-D). In fact, among the 20 most significative altered genes, nine are linked to muscle contraction (*RYR1, TTN, MYH3, MYH2, ACNT2, ATP2A1, MYL1, TNNC2, MYOM3*) are upregulated by Nr2f6 knockdown (Figure 1A). Accordingly, a panel of canonical markers of muscle differentiation containing muscle regulatory factors (MRFs) and myosin isoforms (Figure 1E) reveals that the Nr2f6 knockdown enhanced C2C12 differentiation. Indeed, data generated in our transcriptomic analysis was correlated with a publicly available C2C12 myogenesis dataset (Supplementary Figure 1B). Consistently, the proteins coded by the upregulated genes belonged mostly to the sarcomere, contractile fiber, and cytoplasm location ontologies. Since both an increase in cellular oxidative capacity and the activation of the PI3K pathway are required for myogenesis[25], [26], we verified whether genes of the main pathways of regulation of glycolysis and fatty acid oxidation were affected and found that several energy sensors such as *AKT2*, *PRKAG3* subunit of AMPK, and mTOR complex were upregulated by Nr2f6 loss-of-function (Figure 1F). Myogenic differentiation demands the withdrawal of the cell cycle and both processes are regulated in a concerted manner[27], [28]. Accordingly, the downregulated genes were related to different phases of cell division, with the enrichment of proteins related to DNA replication, packaging, and chromosome separations. Of note, essential components of the cell cycle progression such as *CDC25B/C* phosphatases and *CDK1/4* kinase promote quiescence and halt cell cycle progression in muscle progenitors when down-regulated[29]–[31]. Altogether, the changes in the myocyte's global transcriptome indicate that Nr2f6 inhibits myoblast differentiation and metabolism. Considering the differences between mouse and human myogenic cell's transcriptional landscape[32] we verified whether the result of Nr2f6 depletion in differentiation markers would be translatable to human primary human skeletal muscle cells. We found that expression of *MYH1/2/7*, muscle creatine kinase, and myosin light chain kinase 1 were upregulated in human cells (Figure 1G), indicating a conserved role for Nr2f6 as repressor of myogenesis.

**Increase in cell oxidative capacity by Nr2f6 knockdown.**

Given the enrichment of genes of oxidative metabolism, we first sought to verify the functional effects of Nr2f6 knockdown on metabolism. Oxygen consumption assays (Figure 2A), using palmitate as the major substrate for energy production, provided evidence that Nr2f6 knockdown promoted an increase in maximal respiration capacity after the addition of the uncoupler (carbonyl cyanide m-chlorophenyl hydrazone) CCCP and the spare capacity. Although there was no difference between control and knockdown respiratory parameters in high-glucose media (Supplementary Figure 2A, B), the extracellular acidification rates were reduced, without a reduction of total ATP pool, which was confirmed by lower lactate concentration in knockdown cells (Figure 2B, C, S2C). These results are supported by alterations in the expression of the pyruvate carboxylase, insulin-dependent glucose transporter, and fatty acid transporters (Figure 2D, E). Together, these results indicate Nr2f6 knockdown increases pyruvate and acetyl-CoA flux to the mitochondria, which could be reinforced by upregulation of the glucose transporter *GLUT4*, the anaplerotic enzyme pyruvate carboxylase (PC), and fatty-acid transporters. Our analysis of ENCODE chromatin immunoprecipitation-sequencing (ChIP-seq) data for Nr2f6 in K562 and HepG2 cells indicates an increase in mitochondrial genes related to lipid metabolism (Supplementary Figure 1C). We also identified significant enrichment of kinases related to the insulin signaling pathway when analyzing genes affected by Nr2f6 knockdown in the RNA-seq data and genes with Nr2f6 binding within the promoter region in ENCODE with ChIP-seq data (Supplementary Figure 1C, D). Considering the increase in the efficiency of the Nr2f6 silenced myocytes to oxidize lipids, we hypothesized that depletion of Nr2f6 would be protected against lipid overload in skeletal muscle. Stable Nr2f6 knockdown in myotubes protected (50%) against palmitate-induced cell death and reduced mitochondrial superoxide production (40%) and decreased cytosolic reactive oxygen species (20%) (Figure 2F, G, H). Since Nr2f6 knockdown can increase lipid handling capacity by upregulating mitochondrial and cytosolic lipid transporters, mitochondrial proteins, and TCA cycle anaplerotic genes, thereby increasing oxygen consumption, we verified whether Nr2f6 is modulated by palmitate treatment *in vitro* and by high-fat diet *in vivo* in rodents[33], both pathophysiological conditions of increased lipid

oxidation and supply (Figure 2I-K, S2D, E). Our findings demonstrate that Nr2f6 expression is consistently reduced under these conditions, indicating a role as an energy stress response gene that facilitates metabolic adaptations to lipid oxidation. Collectively, the data provide evidence that Nr2f6 inhibition protects against lipid overload by increasing lipid handling capacity in skeletal muscle.

**Nr2f6 directly represses PGC-1α and UCP3 expression.**

We recently provided evidence that the transcriptional regulation of *UCP3* by the peroxisome proliferator-activated receptor γ co-receptor 1-α (PGC-1α) is essential for the maintenance of myotube viability during lipid overload, by preventing the production of reactive oxygen species (ROS) [34], [35]. Considering a similar phenotype by Nr2f6 knockdown in myotubes, we investigated whether Nr2f6 regulates the same pathway. We found that Nr2f6 overexpression reduced both *UCP3* and *PGC-1α* mRNA in myotubes, which also translated to both reduced PGC-1α protein content and expression of its mitochondrial electron transfer chain (ETC) target genes (Figure 3A-B). Using luciferase reporter assays, we observed Nr2f6 overexpression reduced PGC-1α promoter activity, suggesting direct repression. Conversely, Nr2f6 knockdown in C2C12 myotubes increased PGC-1α downstream ETC targets (Figure 3D). Further investigation into the regulation of *UCP3* transcription by Nr2f6 using 7kbp UCP3 promoter reporter plasmid showed a reduction in the luciferase signal by Nr2f6 overexpression and an increase in activity following Nr2f6 knockdown (Figure 3E). We scanned the UCP3 promoter region and found an Nr2f6 response element downstream of the transcription initiation site, which coincided with the open chromatin region and peaks of known the UCP3 transcription factors, Myod1 and Myogenin (Figure 3F), further supporting the notion that Nr2f6 directly repressed *UCP3* expression. The effects of Nr2f6 knockdown on *UCP3* and *PGC-1α* expression could be reproduced in human and mouse primary myotubes (Figure 3G, S3A). UCP3 transcription is regulated by peroxisome proliferator-activated receptors (PPARs) and estrogen-related receptors (ERRs) in skeletal muscle[36], [37], however, Nr2f6 silencing did not change the transactivation of responsive elements (Supplementary Figure 3B). Collectively, our results indicate that Nr2f6 is a bona fide transcription regulator of UCP3

and PGC-1α. Given that UCP3 is a PGC-1α target, these results indicate that Nr2f6 represses *UCP3* expression indirectly by downregulating *PGC-1α* and by directly binding to the *UCP3* promoter region.

**Nr2f6 activates the cell cycle and represses the expression of genes involved in muscle contraction and oxidative metabolism.**

We next explored the effects of Nr2f6 overexpression *in vivo* by electroporation in the *tibialis anterior* muscle of mice, using the contralateral muscle as control, and studied the global transcriptomic changes by microarray. There were 3796 genes within the criteria for differential expression (FDR <0.05, Fold change >2), among which, 1915 were downregulated and 1781 were upregulated, with Nr2f6 overexpression having a major effect on the hierarchical clustering (Figure 4A). Consistent with earlier reports that highlight Nr2f6 as a gatekeeper of the immune system[24], gene ontology analysis of the upregulated genes shows enrichment of biological processes and pathways related to the immune system (Figure 4B). RT-qPCR was used to validate markers modulated in microarray analysis. We found that indicators of lymphocyte activation *CD44*, the marker for macrophage/monocyte activation *CD68*, and the macrophage marker *F4-80* were upregulated in Nr2f6 expressing muscle (Figure 4E). Accordingly, *TGFb*, a potent inhibitor of hematopoietic cell activation, and the marker for endothelial and non-differentiated hematopoietic cells were downregulated, consistent with an increase in the number and activity of immune system-derived cells, indicating that Nr2f6 might activate resident cells of the immune system and/or promote the invasion of circulating cells. Nr2f6 overexpression also increased expression of Myogenin and, to a lesser extent, *MYOD*, however the downstream targets genes myosin heavy chains 1 and 2 decreased (Figure 4D). Downregulated genes were enriched in energetic metabolism pathways, mitochondria, and muscle contraction terms (Figure 4C), reinforcing the functional phenotypes described *in vitro*. Importantly, the hereby proposed Nr2f6 targets, namely *UCP3* and *PGC-1α*, were downregulated by Nr2f6 overexpression (Figure 4F). The lipid transporters *CD36* and *CPT1B*, as well as subunits of the respiratory chain complexes, which were upregulated by Nr2f6 knockdown *in vitro*, were also downregulated by Nr2f6 overexpression. Additionally, the expression of

reactive oxygen species scavengers *SOD1*, *SOD2*, and catalase genes was decreased (Figure 4F). Collectively, these findings support our functional results and indicate mitochondrial function was impaired by Nr2f6 overexpression.

**Nr2f6 inhibits muscle development and contraction.**

Since Nr2f6 overexpression negatively affects the mRNA expression of genes involved in muscle contraction and development, we next investigated whether the Nr2f6 gain-of-function would impair muscle morphology and function by performing immunostaining for myosin heavy chain (MHC) isoforms and *ex vivo* contraction experiments, respectively. Intriguingly, Nr2f6 overexpressing *tibialis anterior* (TA) weighted less and were visually paler compared with control muscle (Figure 5A). Consistent with these observations, Nr2f6 overexpression reduced the total number of fibers (21%), which together with the increase in cell death-related genes (Figure 4B), and the increase in the atrogenes cathepsin and calpain 2[38] (Supplementary Figure 4A), characterizes a state of atrophy (Figure 5B, C). Stratification by fiber type showed that this reduction is particularly due to the decrease in type IIB fibers, which were reduced by 23%, and although there was a tendency to decrease IIX fiber number (Figure 5D), there was no statistical significance in these comparisons or the number of IIA fibers. We then overexpressed Nr2f6 in the *flexor digitorum brevis* (FDB) and performed *ex vivo* contractions to verify alterations in muscle force production and fatigability. Consistent with the immunostaining data, mass-corrected maximal force production was reduced (60%) (Figure 5E), but time to fatigue was unaltered in Nr2f6 overexpressing muscles (Supplementary Figure 4B). Since the *ex vivo* contraction assay surpasses the neuromuscular system by direct electric stimulation, disregarding action potential issues, fatigability is mostly induced by detriments in calcium homeostasis, such as reduced $Ca^{2+}$ sensitivity, sarcoplasmic $Ca^{2+}$ reuptake, and release[39]. Therefore, we cannot exclude the possibility that the time to fatigue is also affected *in vivo* in Nr2f6 gain-of-function models. So far, these findings strongly suggest induction of atrophy, worsened by an inflammatory state and an imbalance between satellite cell proliferation and differentiation.

**Nr2f6 modulates myoblasts' proliferation rates.**

Next, we investigated whether Nr2f6 regulates cell cycle genes and myoblast proliferation. Thus, we compared differentially expressed genes identified in the microarray of the Nr2f6 overexpression in TA muscle with the RNA-seq transcriptomics from C2C12 myocytes after transient Nr2f6 knockdown. We found 706 genes were differentially expressed in both experiments, whereby 446 genes were modulated in opposite directions indicating a direct regulation by Nr2f6 or a conserved effect of Nr2f6 modulation in both models (Figure 6A). We further scanned the promoter regions of these genes consisting of 3 kbp upstream and downstream of the transcription start site, for the Nr2f6 binding motif. We found 206 matches in unique genes, whereby 73 were upregulated and 133 downregulated by Nr2f6 overexpression. The interaction network of these high-confidence targets (Figure 6B) reveals that the most connected genes are upregulated by Nr2f6 overexpression and are mostly related to the cell cycle, which emphasizes the role of Nr2f6 as a promoter of cell division, and further reinforces the dysplastic phenotype observed in the gain-of-function experiments *in vivo*. Investigation of canonical pathways of myogenesis cell proliferation and stemness in Nr2f6 overexpressing TAs (Figure 6C, D) showed that the content of the proliferating cell nuclear antigen (PCNA), an important general marker for cell proliferation[40], was increased by Nr2f6 overexpression. Together with the increase of the muscle-specific satellite cell marker Pax7, and the activation by phosphorylation of the stemness markers GSK3a/b[1], [41], ERK[42], [43], and S6, these results point to an increase in myogenic progenitors and the infiltration of other cell types, such as cells of the immune system. Nr2f6 overexpression and knockdown can promote or inhibit cell proliferation in cancer cells, respectively[44]–[46]. Our doubling time experiments (Figure 6E, G) confirm this effect is also conserved in C2C12 myoblasts, with an increase of 4 hours in the average doubling time in knockdown cells and a decrease of 3.5 hours in Nr2f6 overexpression stable cell lines. Moreover, RT-qPCR validation of major markers of cell cycle progression inhibitors *RB1* and *P21* show an increase in both genes by Nr2f6 knockdown and a tendency towards downregulation of *RB1* by Nr2f6 overexpression (Figure 6F, H). Collectively, these

results indicate that the function Nr2f6 function as an important repressor of cell cycle progression is conserved in muscle models.

## DISCUSSION

Numerous nuclear receptors are necessary for the maintenance of muscle mass[47], [48]. For example, whole-body knockout of Nr1d1 (Rev-ERBα, Ear-1) leads to an increase in atrophic genes, a decrease in muscle mass, and a relative increase in low-diameter fibers[49]. More broadly, muscle-specific knockout of the nuclear receptor co-repressor 1 (NCoR1) leads to skeletal muscle hypertrophy and increased oxidative metabolism[50]. Here, we found evidence that a disruption in myogenesis also follows Nr2f6 overexpression *in vivo* and *in vitro,* and myoblast proliferation rates are increased. Remarkably, Nr2f2 (COUP-TFII), an Nr2f6 interactor, is among the few nuclear receptors found to promote muscle wasting[51], [52]. However, Nr2f2 expression in myogenic progenitors impairs muscle differentiation in mice by directly repressing genes related to myoblast fusion and proliferation[53], [54], implying that myogenesis is disrupted in a different stage. Future studies should address the redundancy of these NRs in muscle function.

Most of the transgenic and knockdown models provide evidence to suggest that nuclear receptors are involved in a general activation of oxidative metabolism[47]. For example, the muscle-specific Nr4a3 transgenic mouse displays a marked increase in mitochondrial density and fast-to-slow fiber switch[55]. This general rule is reinforced by the fact that mice lacking nuclear receptor co-activators, such as PGC-1α and MED1[56], or overexpressing the co-repressor RIP140[57], have decreased mitochondrial density and fewer oxidative fibers. Conversely, here we show that Nr2f6 is an exception to this model in skeletal muscle since this nuclear receptor can directly reduce PGC-1α and UCP3 promoter activity, thereby increasing the susceptibility of muscle cells to lipid overload by reducing fatty-acid oxidation and increasing reactive oxygen species production. Transgenic mouse models overexpressing UCP3 in muscle are consistently reported to have improved glucose homeostasis under chow and high-fat diet (HFD) conditions, as well as resistance to obesity-induced diabetes[58]–[60]. Moreover, increased

levels of circulating lipids increase UCP3 expression[61], [62]. Here, we demonstrate that direct fatty-acid exposure in C2C12 myotubes or conditions of increased β-oxidation *in vivo* reduces Nr2f6 mRNA expression and protein content, further reinforcing the finding that Nr2f6 mediates the positive effects of UCP3 under physiological conditions. Importantly, we show that the regulation of *UCP3* and *PGC-1α* expression by Nr2f6 is conserved in human skeletal muscle cells.

Sarcopenia is the age-related loss of muscle mass and function, with the reduction of the number and size of myofibers, a switch from type II to I fibers[63], and an underlying mitochondrial dysfunction[64]. This phenotype is closely reproduced by Nr2f6 overexpression in skeletal muscle. In contrast to most members of the NR family, Nr2f6 overexpression not only induces a sarcopenic-like phenotype, with loss of muscle mass and inflammation but also reduces muscle strength and affects energy metabolism. Interestingly, Nr2f6 is upregulated 2-fold in skeletal muscle hereditary spastic paraplegia[65], a disease characterized by progressive lower limb muscle weakness, sometimes accompanied by mitochondrial dysfunction and morphological fiber defects[66], [67]. While additional experiments are warranted to assess the effects of Nr2f6 ablation *in vivo*, Nr2f6 knockdown in myotubes increases myosin heavy chain expression and improves mitochondrial function, suggesting that inhibition of Nr2f6 might be efficacious in the treatment of sarcopenia or other myopathies. Nr2f6 agonists have been proposed as a possible treatment for colitis[68], but based on our finding that Nr2f6 gain-of-function alone provokes muscle loss, the use of such agonists should be further evaluated for the treatment of patients suffering from myopathies and cachexia. Considering the known effects of Nr2f6 in the inflammatory response, the atrophic phenotype may be supported by a role of Nr2f6 in immune cells. Nonetheless, the antagonistic transcriptional changes induced by Nr2f6 overexpression *in vivo*, and knockdown *in vitro* strongly indicate a direct action of Nr2f6 in the myofibers as the major driver of the functional changes.

A conceivable model elucidating the mechanism by which Nr2f6 overexpression culminates in a reduction of muscle force production (Figure 7), entails the downregulation of genes engaged in various

facets of muscle contraction, such as muscle structure, calcium cycling, and action potential. Notably, a few of these genes constitute high-confidence targets. The ryanodine receptor 1 (*RYR1*) is a major component of the calcium release complex, which permits calcium efflux from the sarcoplasmic reticulum into the cytosol. As such, *in vivo* knockdown and mutations of *RYR1* can cause severe myopathies[69]. Other putative targets including myosin light chain kinase 4 (*MYLK4*) and myomesin 1 (*MYOM1*) are downstream of the androgen receptor (AR), which mediates the effects on muscle force production[70]. Interestingly, we found that the spermine oxidase gene (*SMOX*), another important target of the AR in muscle[71], [72] is downregulated by Nr2f6 overexpression *in vivo*, upregulated by Nr2f6 silencing in C2C12 myocytes, and contains Nr2f6 binding motifs at the promoter region. The direct link between Nr2f6 and the spermine synthesis pathway and a possible interaction with the AR warrant further studies.

Targeted studies provided evidence that Nr2f6 activates gene expression by tethering to the promoters of *circRHOT1*[73], *DDA1*[74], and *CD36*[10], and represses the expression of numerous others such as *IL17*, *IL21*, Renin, and Oxytocin[44], [45], [75], [76]. More broadly, our transcriptomics experiments display an equilibrated number of genes up- and downregulated, further implying that Nr2f6 is a dual-function transcription factor. Interestingly, Nr2f6 is a target of MiR-142-3p[77], raising the possibility that miRNAs, besides protein partners and post-translational modifications[44], might aid in the regulation of Nr2f6 activity. Further studies should help to elucidate the mechanism by which Nr2f6 acts as a repressor or activator of gene expression. The case of CD36 illustrates context-dependent regulation given that this gene is activated in the liver[10], but repressed in skeletal muscle by Nr2f6 in mice and humans. This finding suggests that Nr2f6 may be bound to DNA but kept in a repressive state by post-translational modifications or interaction partners, such as RAR Related Orphan Receptor γ (RORγ), another regulator of *CD36* transcription in muscle[78] and liver[79]. In Th17 lymphocytes, Nr2f6 can compete with RORγ for binding at the *IL17* promoter, maintaining the repressive state. This relationship may also be present in skeletal muscle.

As reported for other cell types[11], Nr2f6 also modulates myoblast proliferation *in* vitro and increases the expression of proliferation markers such as *PCNA* and *KI67 in vivo*. In Nr2f6 overexpressing muscle, Myogenin expression is also increased. However, the myosin heavy chains and other indicators of terminally differentiated myofibers are sharply reduced. These findings raise the possibility that the Nr2f6-overexpressing myoblasts proliferate but fail to assemble into robust myofibrils due to a dysregulated temporal modulation of the MRFs during myogenesis, which critically impairs muscle fiber formation and force production. Key regulators of cell cycle cyclin B1 and Cdk1 are placed among high-confidence direct targets of Nr2f6. Cyclin B1 interacts with Cdk1 and is necessary for kinase activity[80] and progression through the G2 mitotic phase. Moreover, Ccnb1 overexpression is increased in several cancer types and ectopic expression increases cell proliferation rates [81], [82]. The simultaneous effect of Nr2f6 modulation on cell cycle and differentiation markers might also be sustained indirectly by the expression of the retinoblastoma protein, which is responsible for cell cycle arrest through the inhibition of the E2F family of transcription factors. In a feedback loop, E2F TFs antagonize MyoD1, which induces Rb expression, thereby linking processes of proliferation and differentiation[83], [84].

Our findings provide evidence that Nr2f6 plays a critical role in the regulation of several aspects of muscle biology. Nr2f6 modulation alone can determine myoblast proliferation rates, consolidating its role as a major regulator of cell cycle progression. In summary, we report that Nr2f6 is a novel regulator of muscle contraction and metabolism, which may hold promise as a possible strategy for the treatment of muscle wasting and metabolic diseases.

## MATERIALS AND METHODS

The main reagents, tools, and models necessary for replicating the reported results are listed in Supplementary Table 2.

**Cell culture** Human primary skeletal muscle cells were isolated from healthy female and male donors (Al-Khalili et al. 2004), age 55 ±5 years old, BMI 25.6 ±1.5 kg.m$^{-2}$. Myoblasts were maintained in

Growth Media (DMEM/F12 High Glucose (Gibco, #31331093) supplemented with 10 mM HEPES (Gibco #15630-056), 16% Fetal calf serum (Sigma, #F7524), and antibiotics (Gibco #15240-062) and differentiated at the confluence with fusion media (74% DMEM High Glucose (Gibco, 31966-021), 20% 199 Medium (Gibco #31150-022), 20 mM HEPES, antibiotics, 0.03 µg/mL Zinc Sulfate (Sigma #Z4750), 1.4 mg/mL Vitamin B12 (Sigma #V6629), and 2% Fetal Calf Serum) supplemented with 100ug/mL Apotransferrin (Biotechne #3188-AT-001G) and 1.7 mM Insulin (Actrapid Penfill, Novo Nordisk #13509) before use. After 5 days of fusion, apo transferrin and insulin were removed from the media, and cells were incubated for 4 more days. Cells were cultivated in a humidified atmosphere containing 7.5% $CO_2$ and regularly tested for mycoplasma. C2C12s, MEFs, and HEK cells were maintained in DMEM High Glucose (Gibco, 31966-021) supplemented with 4 mM L-glutamine, 10% fetal bovine serum, 1 mM sodium pyruvate, and antibiotics. Fetal bovine serum was substituted by 2% horse serum to induce myogenesis in C2C12 cells when 90-100% confluence was reached, and experiments were performed 5 days later.

**Primary mouse skeletal muscle cells** Mice's primary skeletal muscle cells were isolated from wild-type C57Bl6/JUnib as described (Araujo et al. 2020). After euthanasia, hindlimb muscles were dissected and digested with collagenase II, trypsin, and DNAse I. Cells were sifted through a 70 µm cell strainer and plated in 0.1% Matrigel-coated plates. Myoblasts were maintained for 2 days in DMEM High Glucose supplemented with 2 mM L-glutamine, 10% fetal bovine serum, 10% horse serum, 1 mM sodium pyruvate, and antibiotics. Myogenesis was induced by removing fetal bovine serum from the media when confluence was reached, and cells were cultivated for 5 more days. The experiments were approved by the Ethics Committee on Animal Use (CEUA/Unicamp #5626-1/2020).

**Animals** All electroporation experiments were conducted following the guidelines of animal welfare and were approved by the Stockholm North Animal Ethical Committee (Stockholm, Sweden). Male C57Bl6/J mice were acquired from Jackson Labs and maintained at 12/12h light/dark cycle under controlled temperature and humidity, and *ad libitum* access to food (Specialized Research Diets, #

801722) and water. The use of animals for high-fat diet experiments was approved by the Ethics Committee on Animal Use (CEUA/Unicamp #5626-1/2020) and all the welfare guidelines of the National Council of Control of Animal Experimentation (CONCEA) were followed. Male C57Bl6/JUnib mice were kept under the same conditions described above. Mice were provided a high-fat diet (PragSolucoes #0015, 60% kcal from lipids) at 4 weeks of age for 16 weeks; littermates were fed a standard chow diet as a control.

**Reactive oxygen species measurement** Cells were incubated with 5 nM MitoSOX (Invitrogen, #M36008) or 5 µM Dihydroethidium (DHE, Invitrogen, #D11347) in DMEM without phenol red supplemented with 1 mM Sodium Pyruvate, 4 mM L-glutamine, and 25 mM Glucose for 30 min and washed three times before reading in a plate reader 510/580 nm (ex/em) or 520/610 nm (ex/em) for DHE. Samples were fixed and stained with Crystal Violet for normalization.

**RT-qPCR** Total RNA was extracted from cells with TRIzol (Invitrogen #15596-018) following the manufacturer's instruction and cDNA was synthesized with a High-Capacity Reverse Transcription kit (Applied Biosystems #4368814). cDNA was diluted to 10 ng/µL and 20 ng was used for qPCR reactions. NormFinder (Andersen, Jensen, and Ørntoft 2004) was used to decide the best combination of internal controls among RPL39, PPIA, HPRT, 18S, ACTB, and GAPDH. In the *in vivo* electroporation experiments, gene expression was normalized using HPRT-PPIA geomean with TaqMan probes or HPRT-RPL39 geomean when SYBER green was used. For other experiments, gene expression was normalized with multiplexed HPRT when TaqMan probes were used or with RPL39 when SYBER was used. Relative expression was calculated by the $\Delta\Delta C_T$ method (Livak and Schmittgen 2001) and is expressed as fold change over the indicated control. The primers and probes used are listed in Supplementary Table 1.

**RNA-seq** Total RNA was extracted with TRIzol and the upper phase containing RNA was loaded into RNeasy columns (Qiagen, #74004) after the addition of isopropanol, following the manufacturer's instructions. cDNA libraries were prepared with TruSeq Illumina Total RNA Stranded (Illumina) with

Ribo-zero rRNA depletion (Illumina). Sequencing was outsourced to Macrogen Inc. (Seoul, South Korea) and performed in a HiSeq X (Illumina), producing an average of 50.8 Mreads, 95% above Q30. Sequence trimming and adapter removal were done with Trimmomatic (Bolger, Lohse, and Usadel 2014) with the following modifications: HEADCROP = 10, MINLEN = 20, AVGQUAL = 20. Reminiscent reads were aligned to the mouse genome (Ensembl GrCm38) with RNA Star 2.7.2b and gene-level counts were calculated with featureCounts v1.6.4. Differential expression was performed with EdgeR with TMM normalization and p-value adjustment using Benjamini and Hochberg normalization with a 0.05 false discovery rate (FDR) cut-off. The Galaxy platform was used to process all data. Pathway enrichment analysis was done in g:Profiler with an FDR cutoff of 0.01. Interaction networks were generated by String.db and analyzed with CytoScape v3.8 using the EnrichmentMap plugin.

**Palmitate treatment** Palmitate (Sigma, #P5585) in absolute ethanol was conjugated with 1% fatty-acid-free bovine serum albumin (Sigma, #A7030) in cell media for 15 min at 55 $^{o}$C to a 500 µM final concentration. Cells were treated with fresh solutions of palmitate or vehicle (1%BSA, 1% ethanol) for 20 hours.

**Promoter transactivation assays** Luciferase reporter assays were performed in MEF cells transfected with a UCP3 reporter plasmid (Harmancey et al. 2015) (UCP3 EP1, Addgene #71743) or PGC-1α 2kb promoter (Handschin et al. 2003) (Addgene #8887), normalization plasmid coding for *Renilla* luciferase (pRL-SV40) and either control empty vector or Nr2f6 coding plasmid (Gift from Dr. Gottfried Baier, Medical University of Innsbruck, Austria) using Lipofectamine 3000. Luciferase activity was measured with DualGlo Luciferase Reporter Assay (Promega, #E2920). For knockdown assays, cells were transfected with siRNAs one day before the transfection of the reporter plasmids.

**siRNA knockdown** C2C12 cells were transfected with 200 nM non-target siRNA (siScr, Qiagen) or siNr2f6 (Sigma) using Lipofectamine RNAiMax (Invitrogen) following manufacturer's instructions concomitantly with the myogenesis media switch. Experiments were performed on the third or fiftieth

day of differentiation. Primary human skeletal muscle cells were transfected at the fiftieth day of differentiation with 5 nM siScr (Ambion) or siNr2f6 (Ambion).

**Stable cell lines** The Nr2f6-myc insert was subcloned from the Nr2f6-myc-flag plasmid into the pBABE-Puro vector using standard PCR with primers spanning the transcription start site and the myc tag. The viral particles for generating the overexpression HEK293T cells were transfected with pCMV-VSVG, pCL-Eco, and the pBABE-Nr2f6-myc or empty vector. For producing viral particles with the knockdown plasmid, HEK293T cells were transfected with packaging vectors pCMV-dR8.2 dvpr, pCMV-VSVG, and pLKO.1-shGFP or shNr2f6 (TRCN0000026147). Cell medium containing virions was collected, filtered at 0.45 µm, and stored at -80 $^{o}$C until further use. Virus concentrations were titrated by the minimal dilution method, C2C12 cells were transduced with 1 MOI, and cells were selected with 2 µg/mL puromycin for 4 days. The clonal selection was performed in the knockdown cells and the clones were validated as indicated. The modified cells and their respective controls were cultivated synchronously under the same conditions.

**Electroporation** Mice were kept under 2% isoflurane-induced anesthesia and the *tibialis anterior* muscles were injected with 30 µL of 1 mg/mL hyaluronidase (Sigma, #H3506). After 2 hours, the lateral and contralateral *tibialis anterior* were injected with 30 µg of either control empty vector pCMV6 or Nr2f6-myc-flag overexpression plasmid (Origene, #MR206083) and 220V/cm were applied in 8 pulses of 20/200 ms on/off (ECM 830 Electroporator, BTX). Terminal experiments were performed 9 days after electroporation with 13 weeks old mice. For electroporation of FDB muscles, after anesthesia 10 µL of 1 mg/mL hyaluronidase were injected into the footpads and after 1 hour, 20 µg of the control or Nr2f6 coding plasmids. Mice rested for 15 minutes and then 75V/cm were applied in 20 pulses of 20/99 ms on/off with the aid of sterile gold acupuncture needles.

**Contraction** Mouse FDB muscles were electroporated as described and dissected 8 days later. With the muscles still attached to the tendons, contraction threads were tied at the most distal and proximal tendons, and the muscles were transferred to contraction chambers containing prewarmed and

continuously oxygenated KHB buffer at 30$^{o}$C. The optimal muscle length was determined, and all subsequent measurements were performed at this length. For maximal force production mice, FDBs were stimulated at 10, 30, 50, 80, 100, and 120 Hz for 1 second and with 0.1 ms pulses. Muscles were left to rest for 5 minutes before starting the fatigue protocol as follows: 0.1 s train duration, 0.3 s train delay, and pulses of 0.1 ms at 50 Hz. The maximal force was evaluated again 5 min after the end of the fatigue protocol to check muscle integrity. Muscles were weighed and protein extraction was performed to normalize. The maximal force was calculated with the difference of the peak force at 120 Hz and the baseline and time to fatigue taken as the time necessary to reach 50% intensity of the first peak.

**MHC Staining** Electroporated *tibialis anterior* muscles were embedded in O.C.T, immediately frozen in nitrogen-cooled isopentane, and stored at -80$^{o}$C until cryosectioning. Muscle slices were blocked (5% Goat serum, 2% BSA, 0,1% sodium azide in PBS) for 3 hours at room temperature and probed with primary antibodies overnight at 4$^{o}$C in a humidified chamber. The slides were washed 3 times with PBS and incubated with Alexa Fluor conjugated secondary antibodies for 2 hours at room temperature. Coverslips were mounted with ProLong antifade Diamond and whole sections were imaged with a fluorescent scanning microscope at 20x magnification.

**Oxygen consumption assays** Oxygen consumption rates (OCR) were measured in a Seahorse XF24 extracellular flux analyzer according to the manufacturer's instructions. The following drugs were used in the assay: 1 μM oligomycin (Oligo), 2 μM carbonyl cyanate m-chlorophenyl hydrazone (CCCP), and 1 μM rotenone/antimycin (Rot./Ant). ATP-linked OCR was calculated by subtracting OCR post oligomycin addition from the OCR measured before. Reserve capacity was determined by subtracting basal from maximal OCR. Non-mitochondrial values were subtracted before all calculations. For fatty-acid oxidation assays, cell media was switched to low glucose 12 hours before the measurements, and cells were equilibrated in KHB supplemented with 1g/L glucose, 4 mM L-glutamine, and 1 mM sodium pyruvate for 1 hour. Immediately before the assay, BSA-conjugated palmitate was added to a final concentration of 200 μM, and the drugs were added in the same manner. During routine oxygen

consumption assays, cells were maintained in phenol red-free DMEM, supplemented with 4.5g/L glucose, 4 mM L-glutamine, and 1 mM sodium pyruvate, without sodium bicarbonate.

**Lactate measurement** Cells were grown in 96 well plates and then incubated for 3 h with 50 µL Krebs-Henseleit Buffer (1.2 mM Na2HPO4, 2 mM MgSO4, 4.7 mM KCl, 111 mM NaCl, pH 7.3) supplemented with 25 mM glucose, 1 mM pyruvate, and 4 mM Glutamine. Lactate production was enzymatically quantified as NADH fluorescence (360 nm/460 nm) by the reverse reaction of L-lactate dehydrogenase (Rabbit muscle, L25005KU, Sigma) in a reaction containing 20 µL cell media, 2 µg enzyme, 50 mM Tris, and 625 mM Hydrazine in PBS. Following the assay, the cells were fixed and stained with crystal violet for cell number normalization.

**Western blot** Protein extracts from cells and tissues were obtained with RIPA Buffer (Thermo Scientific, # 89900) and 30 µg loaded into SDS-PAGE gels. Proteins were then transferred to 0.45 µm PVDF membranes, probed with the indicated primary antibodies, and detected with ECL. Band intensities were normalized by Ponceau S intensity and data is shown as fold-change over control.

**Microarray** RNA was extracted with TRIzol and subsequently column-purified using RNeasy Mini Kit (Qiagen). Sample integrity was assessed, and the library was prepared using Affymetrix Whole Transcript (WT) Assay kit probed in CGAS cartridge for Clariom S (mouse) following manufacturer's instructions. Total RNA quality was assessed by Agilent Technologies 2200 Tapestation and concentrations were measured by NanoDrop ND-1000 Spectrophotometer. Total RNA (150 ng) was used to generate amplified sense strand cDNA targets using GeneChip® WT Plus Reagent Kit (ThermoFisher Scientific) followed by fragmentation and labeling. 2.3 µg of ss cDNA target was hybridized to Clariom™ S Mouse Arrays for 16 hours at 45°C under rotation in Affymetrix Gene Chip Hybridization Oven 645 (ThermoFisher Scientific). Washing and staining were carried out on Affymetrix GeneChip® Fluidics Station 450 (ThermoFisher Scientific), according to the manufacturer's protocol. The fluorescent intensities were determined with Affymetrix GeneChip Scanner 3000 7G (ThermoFisher Scientific). Transcriptome Analysis Console (TAC) software (v4.0.3, ThermoFisher

Scientific) was used for the analysis of microarray data. Signal values were log2-transformed, and quantile normalized using the Signal Space Transformation (SST-RMA) method. Paired comparisons of gene expression levels between sample groups were performed using moderated t-test as implemented in BioConductor package limma. Gene ontology enrichment tests were performed with g:profiler excluding electronic annotations.

**Cell-death assays** Cell-death assays were performed as described (Lima and Silveira 2018), with slight modifications. Propidium iodide was added to a concentration of 5 µg/mL in cell culture media and incubated for 20 minutes. Hoechst 33342 was then added to a final concentration of 1 µg/mL and samples were incubated for another 10 minutes. Fluorescence was measured at 530/620 nm (ex./em.) and 350/460 (ex./em.) nm in a plate reader.

**Cell doubling time** Cells ($10^4$ ) were plated in four replicates in 12-well plates. Thereafter, cells were collected every 24 hours using trypsin and counted in a Neubauer chamber. The normalized data of three independent experiments were used to obtain the doubling-time regression curve with the initial number constraint.

**ATP measurement** Cells were grown in opaque 96-well white plates and then processed according to the manufacturer's instructions of the CellTiter-Glo® Luminescent Cell Viability Assay kit (Promega). The standard curve of ATP was determined in parallel for absolute quantitation.

**Bioinformatic analysis of public datasets** Nr2f6 ChIP-seq bigwig files from the ENCODE project (GSM2797593 and GSM2534343) available on GEO were used. Using the Galaxy platform, the anchoring position matrix was generated using the compute matrix command from the deeptools package, relative to human genome annotations extracted from the UCSC Genome Browser in bed format. The heatmap was obtained using the plotheatmap tool, also from the deeptools package. Pathway enrichment was analyzed using the g.profiler program (https://biit.cs.ut.ee/gprofiler/gost), with a significance threshold of 0.01 using the g:SCS parameter, without considering electronic term annotations. The correlation in Supplementary Figure 1B was produced with fold-changes of

differentially expressed genes from RNA-seq (FDR <0.05) and fold-change values (expression in myotube/expression in myoblast) from the C2C12 cell differentiation array (GSE4694) considering a p-value cut-off of 0.01, according to GEO2R. UCP3 genome locus in Figure 3E was extracted from the UCSC genome browser with the ChIP-seq tracks of Myogenin (wgEncodeEM002136, wgEncodeEM002132), MyoD (wgEncodeEM002127, wgEncodeEM002129), H3K4me (wgEncodeEM001450), H3K27Ac (wgEncodeEM001450) and DNA hypersensitivity track (wgEncodeEM003399) over NCBI37/mm9 mouse genome assembly.

**Statistical analysis and quantification**

GraphPad Prism v7.0 was used for plotting the data and for statistical analysis. Cell culture experiments were performed independently several times with 3-4 technical replicates. Ratio paired comparison using Student's t-test was used for the analysis of human cells and electroporation experiments, otherwise, an unpaired comparison was chosen, and in both cases, a 0.05 p-value cutoff was used. Details for microarray and RNA-seq statistics are described in their respective methods section and further statistical details are presented in figure labels.

**Acknowledgments**

We would like to appreciate the technical support of Ann-Marie Petterson.

**DECLARATIONS**

**Ethics approval and consent to participate**

All animal experiments were approved by the local regulatory entities, either the Stockholm North Animal Ethical Committee or by the Ethics Committee on Animal Use (CEUA/Unicamp #5626-1/2020), observing the welfare guidelines of the National Council of Control of Animal Experimentation (CONCEA). Consent to participate not applicable.

**Consent for publication**

Not applicable.

## Availability of data and materials

The materials originally produced in this study are available upon request to the lead contact. The transcriptomic data generated in this study can be accessed at the GEO (GSE229102 and GSE228202).

## Competing interests

The authors declare no competing interests

## REFERENCES


[1] Z. Ma, Z. Zhong, Z. Zheng, X. M. Shi, and W. Zhang, "Inhibition of glycogen synthase kinase-3β attenuates glucocorticoid-induced suppression of myogenic differentiation in vitro," *PLoS One*, 2014, doi: 10.1371/journal.pone.0105528.

[2] D. Duan, N. Goemans, S. Takeda, E. Mercuri, and A. Aartsma-Rus, "Duchenne muscular dystrophy," *Nature Reviews Disease Primers.* 2021. doi: 10.1038/s41572-021-00248-3.

[3] P. M. Coen, R. V. Musci, J. M. Hinkley, and B. F. Miller, "Mitochondria as a target for mitigating sarcopenia," *Frontiers in Physiology*. 2019. doi: 10.3389/fphys.2018.01883.

[4] J. L. Brown *et al.*, "Mitochondrial degeneration precedes the development of muscle atrophy in progression of cancer cachexia in tumour-bearing mice," *J. Cachexia. Sarcopenia Muscle*, 2017, doi: 10.1002/jcsm.12232.

[5] K. De Bosscher, S. J. Desmet, D. Clarisse, E. Estébanez-Perpiña, and L. Brunsveld, "Nuclear receptor crosstalk — defining the mechanisms for therapeutic innovation," *Nature Reviews Endocrinology*. 2020. doi: 10.1038/s41574-020-0349-5.

[6] and V. A. N. Kumar, Ashok, "Nuclear receptors as potential therapeutic targets in peripheral arterial disease and related myopathy," *FEBS J.*, 2022, doi: 10.1111/febs.16593.

[7] M. Robinson-Rechavi, H. E. Garcia, and V. Laudet, "The nuclear receptor superfamily," *Journal of Cell Science*. 2003. doi: 10.1242/jcs.00247.

[8] K. W. Nettles and G. L. Greene, "Ligand control of coregulator recruitment to nuclear receptors," *Annual Review of Physiology*. 2005. doi: 10.1146/annurev.physiol.66.032802.154710.

[9] V. Klepsch, K. Siegmund, and G. Baier, "Emerging next-generation target for cancer immunotherapy research: The orphan nuclear receptor NR2F6," *Cancers.* 2021. doi: 10.3390/cancers13112600.

[10] B. Zhou *et al.*, "The Nuclear Orphan Receptor NR2F6 Promotes Hepatic Steatosis through Upregulation of Fatty Acid Transporter CD36," *Adv. Sci.*, 2020, doi: 10.1002/advs.202002273.

[11] H. Li *et al.*, “Nuclear orphan receptor NR2F6 confers cisplatin resistance in epithelial ovarian cancer cells by activating the Notch3 signaling pathway,” *Int. J. Cancer*, 2019, doi: 10.1002/ijc.32293.

[12] N. Hermann-Kleiter *et al.*, “Nuclear orphan receptor NR2F6 directly antagonizes NFAT and RORγt binding to the Il17a promoter,” *J. Autoimmun.*, 2012, doi: 10.1016/j.jaut.2012.07.007.

[13] V. Klepsch *et al.*, “Nuclear receptor NR2F6 inhibition potentiates responses to PD-L1/PD-1 cancer immune checkpoint blockade,” *Nat. Commun.*, 2018, doi: 10.1038/s41467-018-04004-2.

[14] Y. Zhao *et al.*, “‘Stripe’ transcription factors provide accessibility to co-binding partners in mammalian genomes.,” *Mol. Cell*, vol. 82, no. 18, pp. 3398-3411.e11, Sep. 2022, doi: 10.1016/j.molcel.2022.06.029.

[15] L. Al-Khalili, D. Krämer, P. Wretenberg, and A. Krook, “Human skeletal muscle cell differentiation is associated with changes in myogenic markers and enhanced insulin-mediated MAPK and PKB phosphorylation,” *Acta Physiol. Scand.*, 2004, doi: 10.1111/j.1365-201X.2004.01259.x.

[16] H. N. Araujo *et al.*, “Regulation of Lin28a-miRNA let-7b-5p pathway in skeletal muscle cells by peroxisome proliferator-activated receptor delta,” *Am. J. Physiol. - Cell Physiol.*, 2020, doi: 10.1152/ajpcell.00233.2020.

[17] C. L. Andersen, J. L. Jensen, and T. F. Ørntoft, “Normalization of real-time quantitative reverse transcription-PCR data: A model-based variance estimation approach to identify genes suited for normalization, applied to bladder and colon cancer data sets,” *Cancer Res.*, 2004, doi: 10.1158/0008-5472.CAN-04-0496.

[18] K. J. Livak and T. D. Schmittgen, “Analysis of relative gene expression data using real-time quantitative PCR and the 2-ΔΔCT method,” *Methods*, 2001, doi: 10.1006/meth.2001.1262.

[19] A. M. Bolger, M. Lohse, and B. Usadel, “Trimmomatic: A flexible trimmer for Illumina sequence data,” *Bioinformatics*, 2014, doi: 10.1093/bioinformatics/btu170.

[20] R. Harmancey, D. L. Haight, K. A. Watts, and H. Taegtmeyer, “Chronic hyperinsulinemia causes selective insulin resistance and down-regulates uncoupling protein 3 (ucp3) through the

activation of sterol regulatory element-binding protein (srebp)-1 transcription factor in the mouse heart," *J. Biol. Chem.*, 2015, doi: 10.1074/jbc.M115.673988.

[21] C. Handschin, J. Rhee, J. Lin, P. T. Tarr, and B. M. Spiegelman, "An autoregulatory loop controls peroxisome proliferator-activated receptor γ coactivator 1α expression in muscle," *Proc. Natl. Acad. Sci. U. S. A.*, 2003, doi: 10.1073/pnas.1232352100.

[22] T. I. Lima and L. R. Silveira, "A microplate assay for measuring cell death in C2C12 cells," *Biochem. Cell Biol.*, 2018, doi: 10.1139/bcb-2018-0005.

[23] M. Warnecke, H. Oster, J. Revelli, G. Alvarez-bolado, and G. Eichele, "Abnormal development of the locus coeruleus in," *Genes Dev.*, 2005, doi: 10.1101/gad.317905.mice.

[24] N. Hermann-Kleiter *et al.*, "The Nuclear Orphan Receptor NR2F6 Is a Central Checkpoint for Cancer Immune Surveillance," *Cell Rep.*, 2015, doi: 10.1016/j.celrep.2015.08.035.

[25] P. Kaliman, F. Viñals, X. Testar, M. Palacín, and A. Zorzano, "Phosphatidylinositol 3-kinase inhibitors block differentiation of skeletal muscle cells," *J. Biol. Chem.*, 1996, doi: 10.1074/jbc.271.32.19146.

[26] P. Rochard *et al.*, "Mitochondrial activity is involved in the regulation of myoblast differentiation through myogenin expression and activity of myogenic factors," *J. Biol. Chem.*, 2000, doi: 10.1074/jbc.275.4.2733.

[27] O. Halevy *et al.*, "Correlation of terminal cell cycle arrest of skeletal muscle with induction of p21 by MyoD," *Science (80-. ).*, 1995, doi: 10.1126/science.7863327.

[28] I. L. De la Serna, K. Roy, K. A. Carlson, and A. N. Imbalzano, "MyoD Can Induce Cell Cycle Arrest but Not Muscle Differentiation in the Presence of Dominant Negative SWI/SNF Chromatin Remodeling Enzymes," *J. Biol. Chem.*, 2001, doi: 10.1074/jbc.M107281200.

[29] Y. Kobayashi *et al.*, "Cyclin-Dependent Kinase 1 Is Essential for Muscle Regeneration and Overload Muscle Fiber Hypertrophy," *Front. Cell Dev. Biol.*, 2020, doi: 10.3389/fcell.2020.564581.

[30] T. Sato, T. Yamamoto, and A. Sehara-Fujisawa, "MiR-195/497 induce postnatal quiescence of

skeletal muscle stem cells," *Nat. Commun.*, 2014, doi: 10.1038/ncomms5597.

[31] J. M. Zhang, Q. Wei, X. Zhao, and B. M. Paterson, "Coupling of the cell cycle and myogenesis through the cyclin D1-dependent interaction of MyoD with cdk4," *EMBO J.*, 1999, doi: 10.1093/emboj/18.4.926.

[32] A. M. Abdelmoez *et al.*, "Comparative profiling of skeletal muscle models reveals heterogeneity of transcriptome and metabolism," *Am. J. Physiol. - Cell Physiol.*, 2020, doi: 10.1152/ajpcell.00540.2019.

[33] I. Casimiro, N. D. Stull, S. A. Tersey, and R. G. Mirmira, "Phenotypic sexual dimorphism in response to dietary fat manipulation in C57BL/6J mice," *J. Diabetes Complications*, 2021, doi: 10.1016/j.jdiacomp.2020.107795.

[34] T. I. Lima *et al.*, "Role of NCoR1 in mitochondrial function and energy metabolism," *Cell Biology International*. 2018. doi: 10.1002/cbin.10973.

[35] T. I. Lima *et al.*, "Opposing action of NCoR1 and PGC-1α in mitochondrial redox homeostasis," *Free Radic. Biol. Med.*, 2019, doi: 10.1016/j.freeradbiomed.2019.08.006.

[36] V. A. Narkar *et al.*, "AMPK and PPARδ Agonists Are Exercise Mimetics," *Cell*, 2008, doi: 10.1016/j.cell.2008.06.051.

[37] P. M. Badin *et al.*, "Exercise-like effects by Estrogen-related receptor-gamma in muscle do not prevent insulin resistance in db/db mice," *Sci. Rep.*, 2016, doi: 10.1038/srep26442.

[38] D. Taillandier and C. Polge, "Skeletal muscle atrogenes: From rodent models to human pathologies," *Biochimie*. 2019. doi: 10.1016/j.biochi.2019.07.014.

[39] D. G. Allen, G. D. Lamb, and H. Westerblad, "Skeletal muscle fatigue: Cellular mechanisms," *Physiological Reviews*. 2008. doi: 10.1152/physrev.00015.2007.

[40] D. R. Dietrich, "Toxicological and pathological applications of proliferating cell nuclear antigen (PCNA), a novel endogenous marker for cell proliferation," *Crit. Rev. Toxicol.*, 1993, doi: 10.3109/10408449309104075.

[41] N. A. M. Pansters *et al.*, “Muscle-specific GSK-3β ablation accelerates regeneration of disuse-atrophied skeletal muscle,” *Biochim. Biophys. Acta - Mol. Basis Dis.*, 2015, doi: 10.1016/j.bbadis.2014.12.006.

[42] I. Michailovici *et al.*, “Nuclear to cytoplasmic shuttling of ERK promotes differentiation of muscle stem/progenitor cells,” *Dev.*, 2014, doi: 10.1242/dev.107078.

[43] N. C. Jones, Y. V. Fedorov, R. S. Rosenthal, and B. B. Olwin, “ERK1/2 is required for myoblast proliferation but is dispensable for muscle gene expression and cell fusion,” *J. Cell. Physiol.*, 2001, doi: 10.1002/1097-4652(200101)186:1<104::AID-JCP1015>3.0.CO;2-0.

[44] N. Hermann-Kleiter *et al.*, “The Nuclear Orphan Receptor NR2F6 Suppresses Lymphocyte Activation and T Helper 17-Dependent Autoimmunity,” *Immunity*, 2008, doi: 10.1016/j.immuni.2008.06.008.

[45] W. J. Olson *et al.*, “Orphan Nuclear Receptor NR2F6 Suppresses T Follicular Helper Cell Accumulation through Regulation of IL-21,” *Cell Rep.*, 2019, doi: 10.1016/j.celrep.2019.08.024.

[46] S. L. Yang *et al.*, “The expression and biological effect of NR2F6 in non-small cell lung cancer.,” *Front. Oncol.*, vol. 12, p. 940234, 2022, doi: 10.3389/fonc.2022.940234.

[47] B. Kupr, S. Schnyder, and C. Handschin, “Role of nuclear receptors in exercise-induced muscle adaptations,” *Cold Spring Harbor Perspectives in Medicine*. 2017. doi: 10.1101/cshperspect.a029835.

[48] S. A. J. Verbrugge, M. Schönfelder, L. Becker, F. Y. Nezhad, M. H. de Angelis, and H. Wackerhage, “Genes whose gain or loss-of-function increases skeletal muscle mass in mice: A systematic literature review,” *Frontiers in Physiology*. 2018. doi: 10.3389/fphys.2018.00553.

[49] A. Mayeuf-Louchart *et al.*, “Rev-erb-α regulates atrophy-related genes to control skeletal muscle mass,” *Sci. Rep.*, 2017, doi: 10.1038/s41598-017-14596-2.

[50] H. Yamamoto *et al.*, “NCoR1 is a conserved physiological modulator of muscle mass and oxidative function,” *Cell*, vol. 147, no. 4, pp. 827–839, 2011, doi: 10.1016/j.cell.2011.10.017.

[51] N. Shimizu *et al.*, "A muscle-liver-fat signalling axis is essential for central control of adaptive adipose remodelling," *Nat. Commun.*, 2015, doi: 10.1038/ncomms7693.

[52] D. Avram *et al.*, "Heterodimeric interactions between chicken ovalbumin upstream promoter-transcription factor family members ARP1 and Ear2," *J. Biol. Chem.*, 1999, doi: 10.1074/jbc.274.20.14331.

[53] H.-J. Lee *et al.*, "Dysregulation of nuclear receptor COUP-TFII impairs skeletal muscle development OPEN", doi: 10.1038/s41598-017-03475-5.

[54] X. Xie, S. Y. Tsai, and M. J. Tsai, "COUP-TFII regulates satellite cell function and muscular dystrophy," *J. Clin. Invest.*, 2016, doi: 10.1172/JCI87414.

[55] M. A. Pearen *et al.*, "The nuclear receptor, Nor-1, markedly increases type II oxidative muscle fibers and resistance to fatigue," *Mol. Endocrinol.*, 2012, doi: 10.1210/me.2011-1274.

[56] W. Chen, X. Zhang, K. Birsoy, and R. G. Roeder, "A muscle-specific knockout implicates nuclear receptor coactivator MED1 in the regulation of glucose and energy metabolism," *Proc. Natl. Acad. Sci. U. S. A.*, 2010, doi: 10.1073/pnas.1005626107.

[57] A. Seth *et al.*, "The Transcriptional Corepressor RIP140 Regulates Oxidative Metabolism in Skeletal Muscle," *Cell Metab.*, 2007, doi: 10.1016/j.cmet.2007.08.004.

[58] C. Son *et al.*, "Reduction of diet-induced obesity in transgenic mice overexpressing uncoupling protein 3 in skeletal muscle," *Diabetologia*, 2004, doi: 10.1007/s00125-003-1272-8.

[59] J. Darcy MacLellan, M. F. Gerrits, A. Gowing, P. J. S. Smith, M. B. Wheeler, and M. E. Harper, "Physiological increases in uncoupling protein 3 augment fatty acid oxidation and decrease reactive oxygen species production without uncoupling respiration in muscle cells," *Diabetes*, 2005, doi: 10.2337/diabetes.54.8.2343.

[60] J. C. Clapham *et al.*, "Mice overexpressing human uncoupling protein-3 in skeletal muscle are hyperphagic and lean," *Nature*, 2000, doi: 10.1038/35019082.

[61] C. Son *et al.*, "Up-regulation of uncoupling protein 3 gene expression by fatty acids and

agonists for PPARs in L6 myotubes," *Endocrinology*, 2001, doi: 10.1210/endo.142.10.8446.

[62] D. S. Weigle *et al.*, "Elevated free fatty acids induce uncoupling protein 3 expression in muscle: A potential explanation for the effect of fasting," *Diabetes*, 1998, doi: 10.2337/diab.47.2.298.

[63] A. J. Cruz-Jentoft and A. A. Sayer, "Sarcopenia," *The Lancet*. 2019. doi: p.

[64] A. Picca *et al.*, "Update on mitochondria and muscle aging: All wrong roads lead to sarcopenia," *Biological Chemistry*. 2018. doi: 10.1515/hsz-2017-0331.

[65] M. Bakay *et al.*, "Nuclear envelope dystrophies show a transcriptional fingerprint suggesting disruption of Rb-MyoD pathways in muscle regeneration," *Brain*, 2006, doi: 10.1093/brain/awl023.

[66] S. Salinas, C. Proukakis, A. Crosby, and T. T. Warner, "Hereditary spastic paraplegia: clinical features and pathogenetic mechanisms," *The Lancet Neurology*. 2008. doi: 10.1016/S1474-4422(08)70258-8.

[67] J. K. Fink, "Hereditary spastic paraplegia: Clinico-pathologic features and emerging molecular mechanisms," *Acta Neuropathologica*. 2013. doi: 10.1007/s00401-013-1115-8.

[68] V. Klepsch *et al.*, "Nuclear orphan receptor NR2F6 as a safeguard against experimental murine colitis," *Gut*, 2018, doi: 10.1136/gutjnl-2016-313466.

[69] L. Pelletier *et al.*, "In vivo RyR1 reduction in muscle triggers a core-like myopathy," *Acta Neuropathol. Commun.*, 2020, doi: 10.1186/s40478-020-01068-4.

[70] I. Sakakibara *et al.*, "Myofiber androgen receptor increases muscle strength mediated by a skeletal muscle splicing variant of Mylk4," *iScience*, 2021, doi: 10.1016/j.isci.2021.102303.

[71] N. K. L. Lee and H. E. Maclean, "Polyamines, androgens, and skeletal muscle hypertrophy," *Journal of Cellular Physiology*. 2011. doi: 10.1002/jcp.22569.

[72] M. Cervelli, A. Leonetti, G. Duranti, S. Sabatini, R. Ceci, and P. Mariottini, "Skeletal Muscle Pathophysiology: The Emerging Role of Spermine Oxidase and Spermidine," *Med. Sci.*, 2018, doi: 10.3390/medsci6010014.

[73] L. Wang, H. Long, Q. Zheng, X. Bo, X. Xiao, and B. Li, "Circular RNA circRHOT1 promotes

hepatocellular carcinoma progression by initiation of NR2F6 expression," *Mol. Cancer*, 2019, doi: 10.1186/s12943-019-1046-7.

[74] J. Liu, T. Li, and X. L. Liu, "DDA1 is induced by NR2F6 in ovarian cancer and predicts poor survival outcome," *Eur. Rev. Med. Pharmacol. Sci.*, 2017.

[75] E. T. Weatherford, X. Liu, and C. D. Sigmund, "Regulation of renin expression by the orphan nuclear receptors Nr2f2 and Nr2f6," *Am. J. Physiol. - Ren. Physiol.*, 2012, doi: 10.1152/ajprenal.00362.2011.

[76] K. Chu and H. H. Zingg, "The nuclear orphan receptors COUP-TFII and Ear-2 act as silencers of the human oxytocin gene promoter," *J. Mol. Endocrinol.*, 1997, doi: 10.1677/jme.0.0190163.

[77] C. Jin, L. Xiao, Z. Zhou, Y. Zhu, G. Tian, and S. Ren, "MiR-142-3p suppresses the proliferation, migration and invasion through inhibition of NR2F6 in lung adenocarcinoma," *Hum. Cell*, 2019, doi: 10.1007/s13577-019-00258-0.

[78] S. Raichur, P. Lau, B. Staels, and G. E. O. Muscat, "Retinoid-related orphan receptor γ regulates several genes that control metabolism in skeletal muscle cells: Links to modulation of reactive oxygen species production," *J. Mol. Endocrinol.*, 2007, doi: 10.1677/jme.1.00010.

[79] J. Iqbal *et al.*, "Deletion of retinoic acid-related orphan receptor gamma reduces body weight and hepatic lipids in mice by modulating the expression of lipid metabolism genes," *Vessel Plus*, 2019, doi: 10.20517/2574-1209.2019.28.

[80] Y. Fang, H. Yu, X. Liang, J. Xu, and X. Cai, "Chk1-induced CCNB1 overexpression promotes cell proliferation and tumor growth in human colorectal cancer," *Cancer Biol. Ther.*, 2014, doi: 10.4161/cbt.29691.

[81] V. Huang *et al.*, "Upregulation of Cyclin B1 by miRNA and its implications in cancer," *Nucleic Acids Res.*, 2012, doi: 10.1093/nar/gkr934.

[82] B. Bao, X. Yu, and W. Zheng, "MiR-139-5p Targeting CCNB1 Modulates Proliferation, Migration, Invasion and Cell Cycle in Lung Adenocarcinoma," *Mol. Biotechnol.*, 2022, doi:

10.1007/s12033-022-00465-5.

[83] V. K. Rao *et al.*, "G9a promotes proliferation and inhibits cell cycle exit during myogenic differentiation," *Nucleic Acids Res.*, 2016, doi: 10.1093/nar/gkw483.

[84] J. D. R. Knight and R. Kothary, "The myogenic kinome: Protein kinases critical to mammalian skeletal myogenesis," *Skeletal Muscle*. 2011. doi: 10.1186/2044-5040-1-29.

[85] H. Tajsharghi and A. Oldfors, "Myosinopathies: Pathology and mechanisms," *Acta Neuropathologica*. 2013. doi: 10.1007/s00401-012-1024-2.

[86] S. Schiaffino, "Muscle fiber type diversity revealed by anti-myosin heavy chain antibodies," *FEBS Journal*. 2018. doi: 10.1111/febs.14502.

## FIGURES LEGENDS

**Figure 1. Nr2f6 knockdown derepresses the expression of genes involved in metabolism and myogenesis. (A)** Volcano plot of Nr2f6 knockdown C2C12 myocytes. Genes upregulated in red and downregulated in blue (FDR <0.05, $\log_2$FC >0.5). N=4-5.**(B)** Network of ontology terms enriched in the differentially expressed genes. Groups of similar terms were manually curated and encircled as indicated. **(C, D)** Gene ontology enrichment of downregulated and upregulated genes. **(E)** Panel of myogenic differentiation markers differentially regulated by Nr2f6 knockdown with Myogenic Regulatory Factors (MRFs) and myosin isoforms with their respective fiber expression pattern[85], [86]. **(F)** Insulin signaling pathway schematic displaying differentially expressed genes after Nr2f6 knockdown and other components of the pathway. Metabolites are depicted in yellow borders and unchanged genes are in orange borders. **(G)** Gene expression measured by RT-qPCR of markers of myogenic differentiation in primary human skeletal muscle cells transfected with control non-target RNAi (siScr) or siNr2f6. N = 5-6. Boxplot with whiskers spanning minimum to maximal and box edges $25^{th}$-$75^{th}$ percentile, the line at the median and + at the mean. * Indicates $p < 0.05$ using unpaired two-tailed Student's t-test.

**Figure 2. Nr2f6 depletion increases fatty acid oxidation and protects cells against lipid-induced stress. (A)** Fatty-acid-dependent oxygen consumption assay in control siScr and siNr2f6 C2C12 myocytes. Data displayed as mean ±SD. On the right, calculated respiratory parameters are displayed as a line on the mean and minimum to max bars. N = 3. * Indicates $p < 0.05$ using unpaired two-tailed Student's t-test. **(B)** Oligomycin-induced extracellular acidification rate during a high-glucose oxygen consumption assay. N=4. **(C)** Lactate measurement in cell culture media of C2C12 myocytes transfected with control siScr and siNr2f6. N=3. **(D, E)** Relative gene expression using RT-qPCR in stable Nr2f6 knockdown (shNr2f6) C2C12 cells and control shGFP stable cells. **(F)** Cell death as measured by propidium iodide in control (shGFP) and shNr2f6 myocytes following treatment with 500 µM palmitate for 20 hours. N=3. **(G, H)** Mitochondrial and total superoxide production following palmitate treatment

in shGFP and shNr2f6 stable C2C12 cells. N=3-4. **(I)** Relative Nr2f6 mRNA expression in C2C12 myotubes treated with 500 µM palmitate or vehicle for 20 hours. N=3. **(J)** Relative Nr2f6 mRNA expression in the gastrocnemius of mice undergoing a control chow or high-fat diet for 16 weeks. N=7. **(K)** Densitometry and representative western blot image of Nr2f6 in gastrocnemius lysates from mice fed HFD or control chow for 16 weeks. N=6. Boxplot with whiskers spanning minimum to maximal and box edges $25^{th}$-$75^{th}$ percentile, the line at the median and + at the mean. * Indicates $p < 0.05$ using unpaired two-tailed Student's t-test.

**Figure 3. Nr2f6 directly regulates PGC1-a and UCP3 gene expression. (A)** Relative gene expression using RT-qPCR in stable Nr2f6-myc overexpression myotubes. N=4-5. **(B)** Densitometry and representative images of PGC-1α western blot in stable Nr2f6-myc overexpression myotubes. N=5. **(C)** Relative gene expression using RT-qPCR in stable Nr2f6 knockdown myotubes. N=3-5. **(D)** Luciferase reporter assay in HEK293 cells with 2 kbp PGC1A promoter overexpressing HA-tagged Nr2f6 or control empty vector (EV). **(E)** Luciferase activity of UCP3 promoter transactivation assay in cells overexpressing Nr2f6-myc and siNr2f6 transfected cells. N=3. **(F)** Mouse UCP3 genomic locus retrieved from UCSC Genome Browser with the Nr2f6 response element highlighted. Top tracks: ChIP-seq of Myogenin and MyoD at 24h and 60h of differentiation. Middle track: DNAse hypersensitivity assay, with open sensitive regions in grey. Bottom tracks: histone marks ChIP-seq. **(G)** Relative gene expression using RT-qPCR in human primary skeletal myotubes transfected with siNr2f6 or siScr. N=6. Boxplot with whiskers spanning minimum to maximal and box edges $25^{th}$-$75^{th}$ percentile, the line at the median and + at the mean. * Indicates $p < 0.05$ using unpaired two-tailed Student's t-test. The numbers above some bars indicate the p-value.

**Figure 4. The molecular signature of Nr2f6 overexpression in skeletal muscle reveals an increase in inflammation and a decrease in muscle contraction and metabolism. (A)** Heat-map of top 30 most modulated genes in *tibialis anterior* muscle electroporated with empty vector (control) or an Nr2f6 coding plasmid. N=4. **(B, C)** Gene ontology enrichment of downregulated and upregulated genes. **(D, E,**

**F)** Validation of selected markers modulated in the microarray by RT-qPCR. N=4. Insert on D: representative western blot for validation of Nr2f6 protein content in *tibialis anterior* samples under control and electroporated conditions. Boxplot with whiskers spanning minimum to maximal and box edges $25^{th}$-$75^{th}$ percentile, the line at the median and + at the mean. * Indicates $p < 0.05$ using unpaired two-tailed Student's t-test. The numbers above some bars indicate the p-value.

**Figure 5. Overexpression of Nr2f6 induces muscle atrophy and impairs muscle force production. (A)** Weight of *tibialis anterior* muscles (TA) electroporated with empty vector or Nr2f6 coding plasmid. Top: representative photo. N=12. **(B)** Representative images of myosin heavy chain staining in the electroporated TAs for fiber type determination. In green, MHC IIA; in red, MHC IIB; unstained fibers as IIX. No significant number of MHCI fibers were stained, therefore the corresponding channel was omitted. N=7. **(C, D)** Total and type-segmented number of fibers. N=7. **(E)** *Ex-vivo* contraction maximal force production in FDB muscles electroporated with control empty vector (EV) or Nr2f6 coding plasmid. N=5. Data are displayed as individual animals and bars at the mean. * Indicates $p < 0.05$ using ratio paired two-tailed Student's t-test.

**Figure 6. Nr2f6 promotes myoblast proliferation. (A)** Scatter plot of differentially expressed genes in Nr2f6 knockdown in C2C12 myocytes and Nr2f6 overexpression in mice TA. In red: genes upregulated by Nr2f6; in blue: genes downregulated by Nr2f6; in grey: genes with the same direction of modulation by Nr2f6 overexpression and knockdown. **(B)** Interaction network of genes consistently regulated by Nr2f6 overexpression and knockdown and with detected Nr2f6 binding motif at the promoter region. In blue: genes downregulated; in red: genes upregulated. The number of connections of each gene increases clockwise. **(C, D)** Representative images of western blot of the electroporated *tibialis anterior* and densitometric quantitation of protein bands. N=4. **(E, G)** Proliferation curves of stable Nr2f6 knockdown and overexpression cell lines and the calculated doubling time. **(F, H)** RT-qPCR of cell cycle arrest markers in Nr2f6 knockdown and overexpression stable cell lines, respectively. N=4-6. Boxplot with whiskers spanning minimum to maximal and box edges $25^{th}$-$75^{th}$ percentile, the line at the

median and + at the mean. * Indicates $p < 0.05$ using unpaired two-tailed Student's t-test. The numbers above some bars indicate the p-value.

**Figure 7. Nr2f6 represses core genes of muscle contraction.** Nr2f6 overexpression reduces the expression of several genes of the contractile apparatus, myofiber calcium handling, and action potential transduction. Genes with Nr2f6 binding motif at the promoter are underscored. Differentially expressed genes following Nr2f6 overexpression in mouse TA were selected according to ontology terms related to muscle contraction and function. The arrows indicate the up- or downregulation. Sodium Voltage-Gated Channel Alpha Subunit 4 (Scn4a), Potassium Inwardly Rectifying Channel Subfamily J Member 2 (Kcnj2), Solute Carrier Family 8 Member A3 (Slc8a3), Muscle Associated Receptor Tyrosine Kinase (Musk), Ryanodine Receptor 1 (Ryr1), Calsequestrin 1 (Casq1), ATPase Sarcoplasmic/Endoplasmic Reticulum Ca2+ Transporting 2 (SERCA2, Atp2a2), Cholinergic Receptor Nicotinic Alpha 1/delta/gamma subunit Chrna1/d/g), Troponin T1/I1/I2/C1 (Tnnt1/Tnni1/Tnni2/c1), Myom1/2 (Myomesin1/2), Myozenin1/3 (Myoz1/3), Myosin light chain kinase 2/4 (Mylk2/4), Myosin heavy chain 3 (Myh3), Myosin binding protein C1/2 (Mybpc1/2)

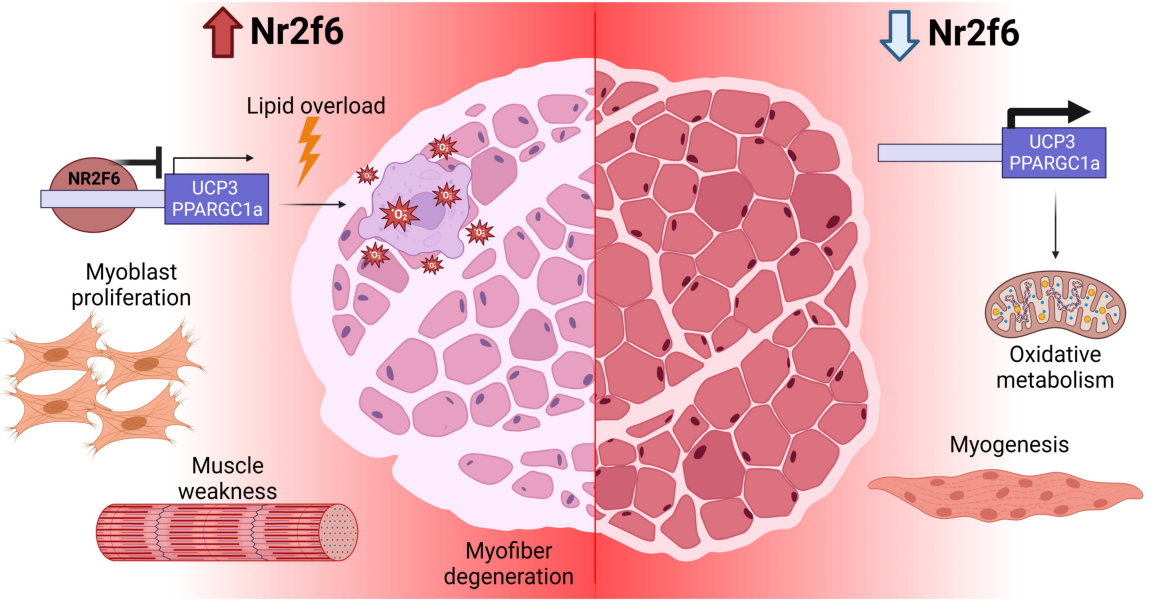
Nr2f6
Nr2f6
Lipid overload
NR2F6
UCP3
PPARGC1a
UCP3
PPARGC1a
Myoblast
proliferation
Oxidative
metabolism
Muscle
weakness
Myogenesis
Myofiber
degeneration

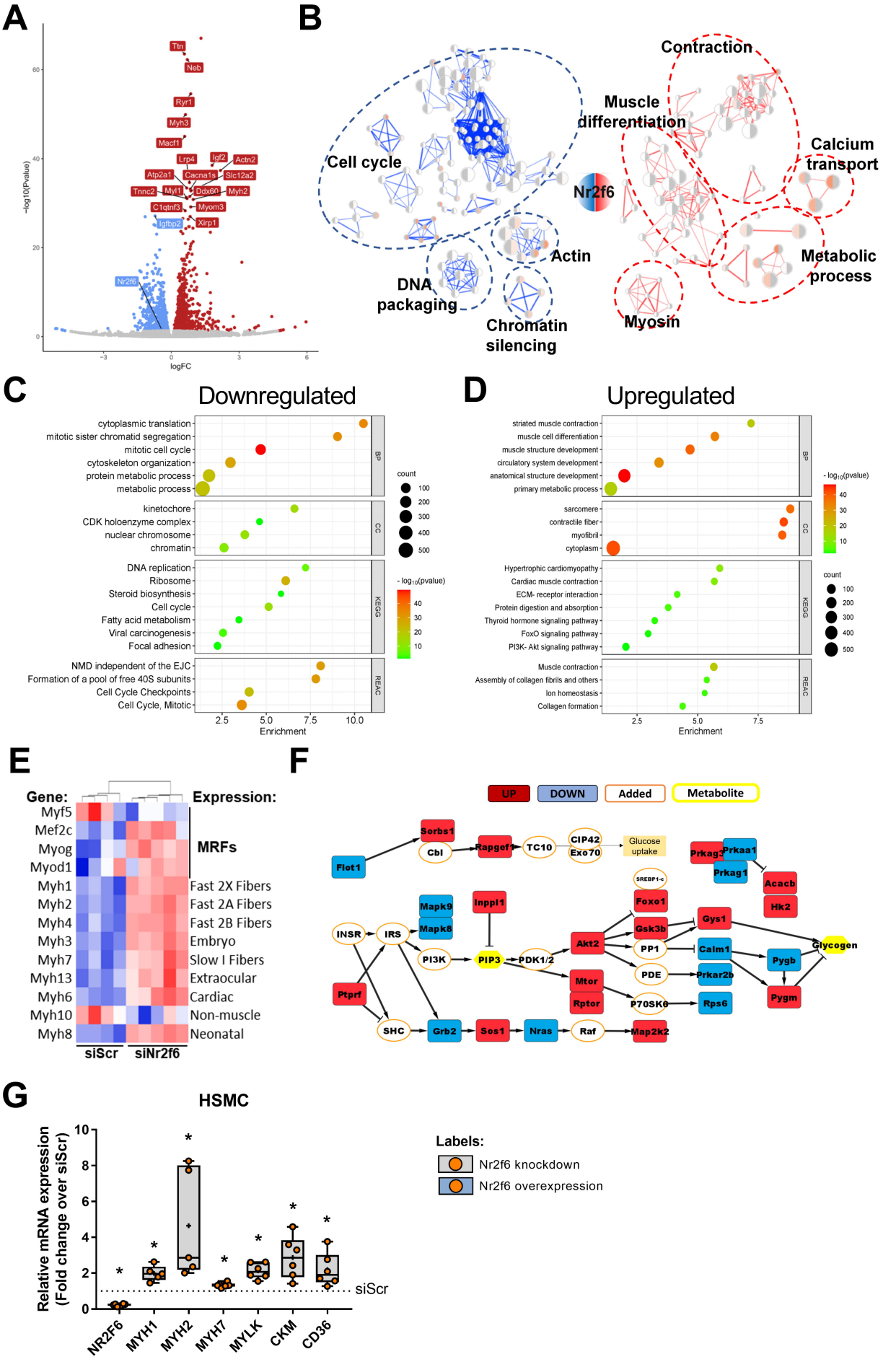
A
Ttn
Neb
Ryr1
Myh3
Macf1
Lrp4
Igf2
Actn2
Atp2a1
Cacna1s
Slc12a2
Tnnc2
Myl1
Ddx60
Myh2
C1qtnf3
Myom3
Igfbp2
Xirp1
Nr2f6
-log10(Pvalue)
logFC
B
Contraction
Muscle differentiation
Calcium transport
Cell cycle
Nr2f6
Actin
Metabolic process
DNA packaging
Chromatin silencing
Myosin
C
Downregulated
cytoplasmic translation
mitotic sister chromatid segregation
mitotic cell cycle
cytoskeleton organization
protein metabolic process
metabolic process
kinetochore
CDK holoenzyme complex
nuclear chromosome
chromatin
DNA replication
Ribosome
Steroid biosynthesis
Cell cycle
Fatty acid metabolism
Viral carcinogenesis
Focal adhesion
NMD independent of the EJC
Formation of a pool of free 40S subunits
Cell Cycle Checkpoints
Cell Cycle, Mitotic
BP
CC
KEGG
REAC
count
- log10(pvalue)
Enrichment
D
Upregulated
striated muscle contraction
muscle cell differentiation
muscle structure development
circulatory system development
anatomical structure development
primary metabolic process
sarcomere
contractile fiber
myofibril
cytoplasm
Hypertrophic cardiomyopathy
Cardiac muscle contraction
ECM- receptor interaction
Protein digestion and absorption
Thyroid hormone signaling pathway
FoxO signaling pathway
PI3K- Akt signaling pathway
Muscle contraction
Assembly of collagen fibrils and others
Ion homeostasis
Collagen formation
E
Gene:
Expression:
Myf5
Mef2c
Myog
Myod1
MRFs
Myh1
Myh2
Myh4
Myh3
Myh7
Myh13
Myh6
Myh10
Myh8
Fast 2X Fibers
Fast 2A Fibers
Fast 2B Fibers
Embryo
Slow I Fibers
Extraocular
Cardiac
Non-muscle
Neonatal
siScr
siNr2f6
F
UP
DOWN
Added
Metabolite
Flot1
Sorbs1
Cbl
Rapgef1
TC10
CIP42
Exo70
Glucose uptake
Prkag3
Prkaa1
Prkag1
Acacb
Hk2
SREBP1-c
Foxo1
Mapk9
Mapk8
Inppl1
INSR
IRS
PI3K
PIP3
PDK1/2
Akt2
Gsk3b
PP1
PDE
Gys1
Calm1
Prkar2b
Glycogen
Pygb
Pygm
Ptprf
Mtor
Rptor
P70SK6
Rps6
SHC
Grb2
Sos1
Nras
Raf
Map2k2
G
HSMC
Relative mRNA expression (Fold change over siScr)
siScr
NR2F6
MYH1
MYH2
MYH7
MYLK
CKM
CD36
Labels:
Nr2f6 knockdown
Nr2f6 overexpression

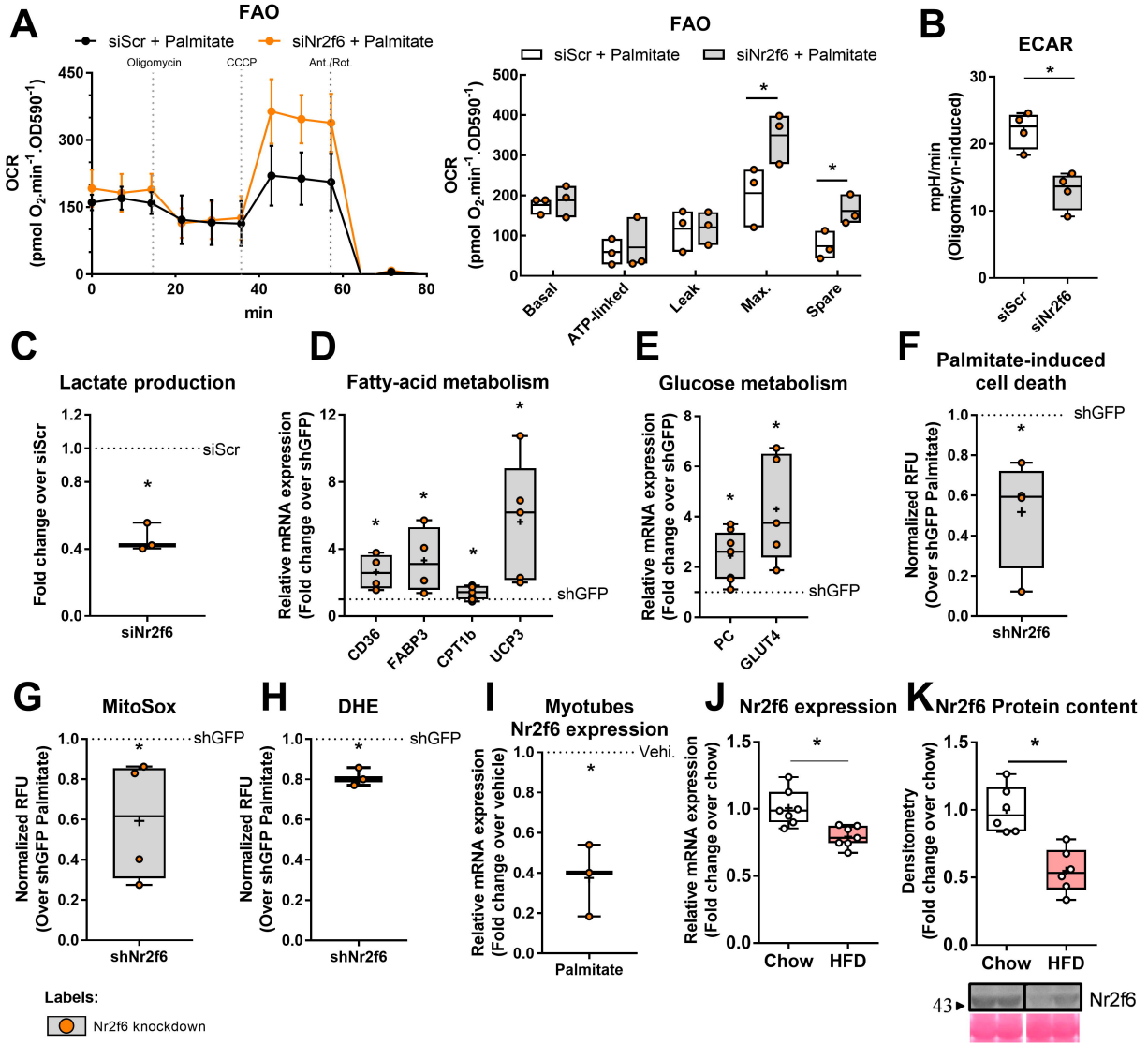
A
FAO
siScr + Palmitate
siNr2f6 + Palmitate
Oligomycin
CCCP
Ant./Rot.
OCR
(pmol O2.min-1.OD590-1)
min
FAO
siScr + Palmitate
siNr2f6 + Palmitate
Basal
ATP-linked
Leak
Max.
Spare
B
ECAR
mpH/min
(Oligomicyn-induced)
siScr
siNr2f6
C
Lactate production
Fold change over siScr
siScr
siNr2f6
D
Fatty-acid metabolism
Relative mRNA expression
(Fold change over shGFP)
shGFP
CD36
FABP3
CPT1b
UCP3
E
Glucose metabolism
Relative mRNA expression
(Fold change over shGFP)
shGFP
PC
GLUT4
F
Palmitate-induced
cell death
Normalized RFU
(Over shGFP Palmitate)
shGFP
shNr2f6
G
MitoSox
Normalized RFU
(Over shGFP Palmitate)
shGFP
shNr2f6
H
DHE
Normalized RFU
(Over shGFP Palmitate)
shGFP
shNr2f6
I
Myotubes
Nr2f6 expression
Relative mRNA expression
(Fold change over vehicle)
Vehi.
Palmitate
J
Nr2f6 expression
Relative mRNA expression
(Fold change over chow)
Chow
HFD
K
Nr2f6 Protein content
Densitometry
(Fold change over chow)
Chow
HFD
43
Nr2f6
Labels:
Nr2f6 knockdown

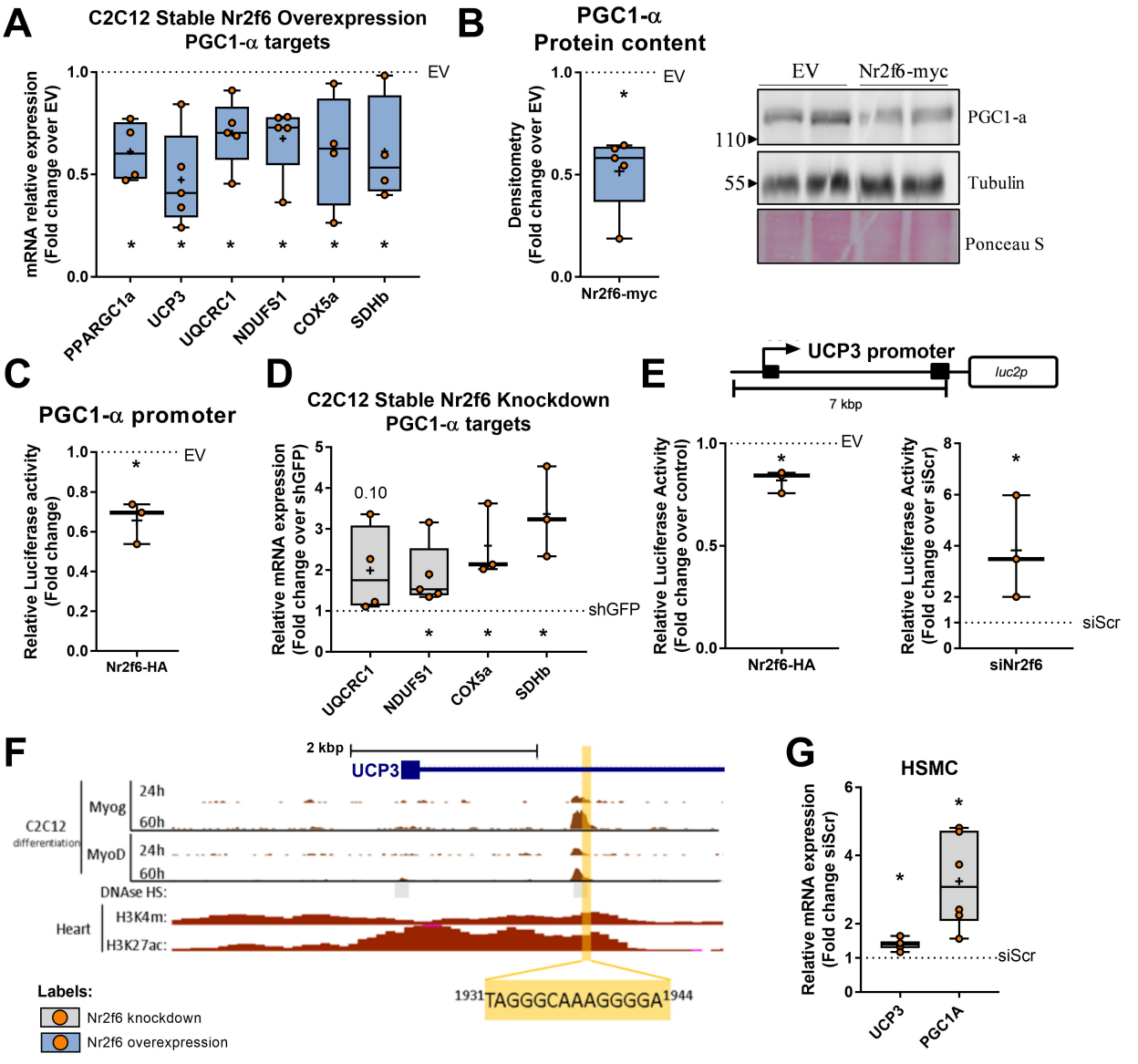
A
C2C12 Stable Nr2f6 Overexpression
PGC1-α targets
mRNA relative expression
(Fold change over EV)
EV
PPARGC1a
UCP3
UQCRC1
NDUFS1
COX5a
SDHb
B
PGC1-α
Protein content
Densitometry
(Fold change over EV)
Nr2f6-myc
EV
Nr2f6-myc
PGC1-a
Tubulin
Ponceau S
110
55
C
PGC1-α promoter
Relative Luciferase activity
(Fold change)
Nr2f6-HA
D
C2C12 Stable Nr2f6 Knockdown
PGC1-α targets
Relative mRNA expression
(Fold change over shGFP)
0.10
shGFP
UQCRC1
NDUFS1
COX5a
SDHb
E
UCP3 promoter
luc2p
7 kbp
Relative Luciferase Activity
(Fold change over control)
Nr2f6-HA
Relative Luciferase Activity
(Fold change over siScr)
siScr
siNr2f6
F
2 kbp
UCP3
C2C12
differentiation
Myog
MyoD
24h
60h
DNAse HS:
Heart
H3K4m:
H3K27ac:
1931 TAGGGCAAAGGGGA 1944
Labels:
Nr2f6 knockdown
Nr2f6 overexpression
G
HSMC
Relative mRNA expression
(Fold change siScr)
siScr
UCP3
PGC1A

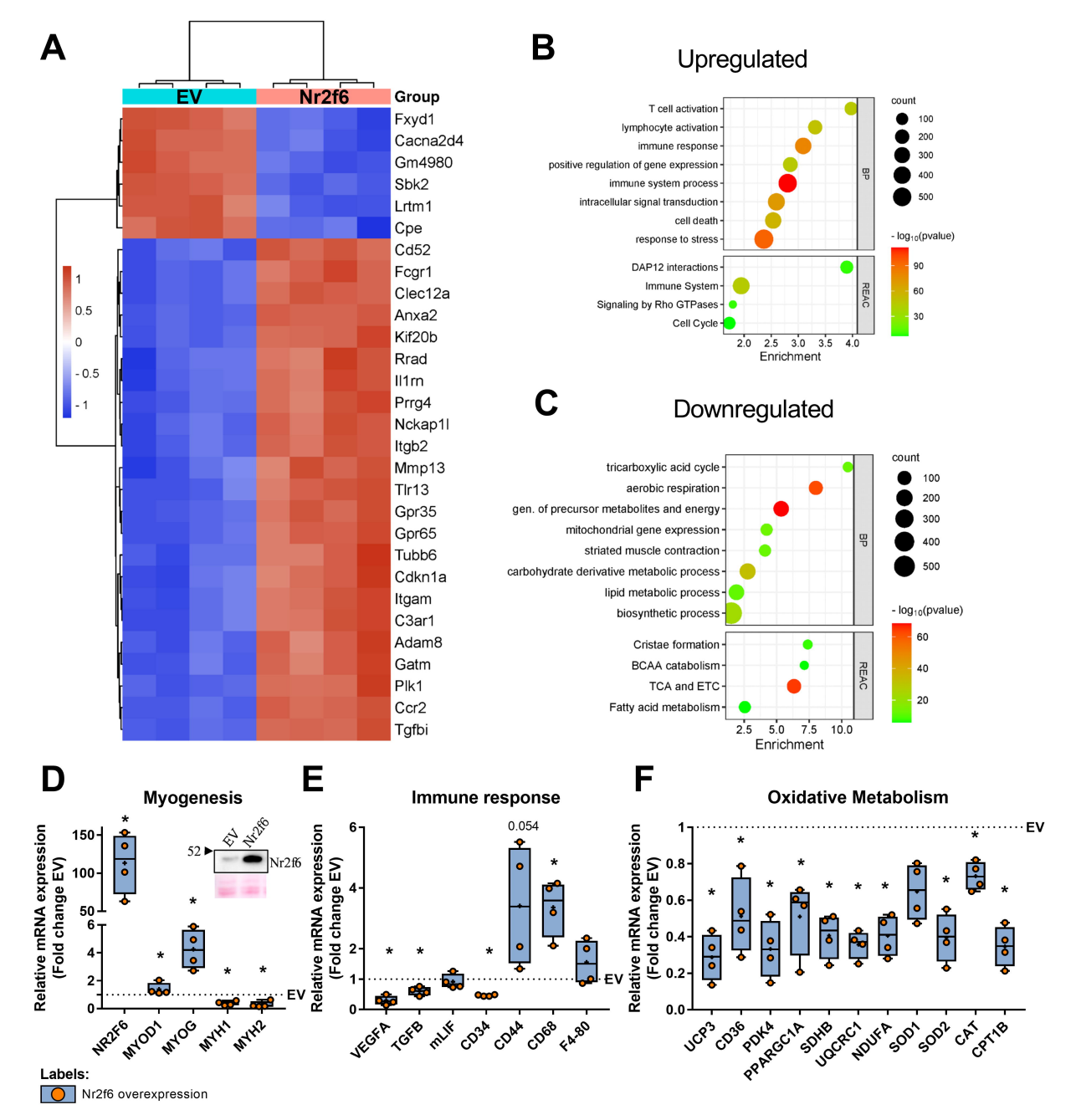
A
EV
Nr2f6
Group
Fxyd1
Cacna2d4
Gm4980
Sbk2
Lrtm1
Cpe
Cd52
Fcgr1
Clec12a
Anxa2
Kif20b
Rrad
Il1rn
Prrg4
Nckap1l
Itgb2
Mmp13
Tlr13
Gpr35
Gpr65
Tubb6
Cdkn1a
Itgam
C3ar1
Adam8
Gatm
Plk1
Ccr2
Tgfbi
1
0.5
0
- 0.5
- 1
B
Upregulated
T cell activation
lymphocyte activation
immune response
positive regulation of gene expression
immune system process
intracellular signal transduction
cell death
response to stress
BP
DAP12 interactions
Immune System
Signaling by Rho GTPases
Cell Cycle
REAC
2.0 2.5 3.0 3.5 4.0
Enrichment
count
100
200
300
400
500
- log10(pvalue)
90
60
30
C
Downregulated
tricarboxylic acid cycle
aerobic respiration
gen. of precursor metabolites and energy
mitochondrial gene expression
striated muscle contraction
carbohydrate derivative metabolic process
lipid metabolic process
biosynthetic process
BP
Cristae formation
BCAA catabolism
TCA and ETC
Fatty acid metabolism
REAC
2.5 5.0 7.5 10.0
Enrichment
count
100
200
300
400
500
- log10(pvalue)
60
40
20
D
Myogenesis
Relative mRNA expression (Fold change EV)
150
100
50
6
4
2
0
EV
52
EV
Nr2f6
Nr2f6
NR2F6
MYOD1
MYOG
MYH1
MYH2
E
Immune response
Relative mRNA expression (Fold change EV)
6
4
2
1
0
0.054
EV
VEGFA
TGFB
mLIF
CD34
CD44
CD68
F4-80
F
Oxidative Metabolism
Relative mRNA expression (Fold change EV)
1
0.8
0.6
0.4
0.2
0.0
EV
UCP3
CD36
PDK4
PPARGC1A
SDHB
UQCRC1
NDUFA
SOD1
SOD2
CAT
CPT1B
Labels:
Nr2f6 overexpression

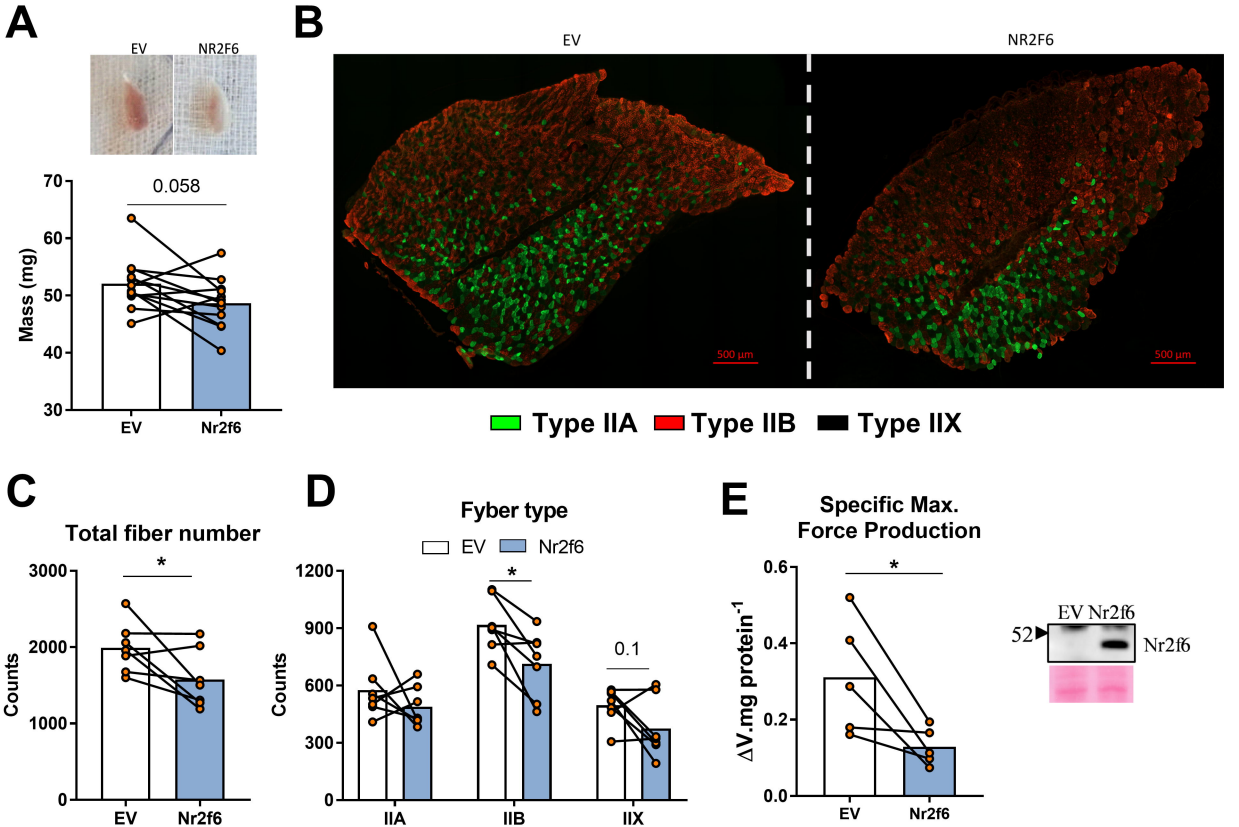
A
EV
NR2F6
0.058
Mass (mg)
70
60
50
40
30
EV
Nr2f6
B
EV
NR2F6
500 µm
500 µm
Type IIA
Type IIB
Type IIX
C
Total fiber number
*
Counts
3000
2000
1000
0
EV
Nr2f6
D
Fyber type
EV
Nr2f6
*
0.1
Counts
1200
900
600
300
0
IIA
IIB
IIX
E
Specific Max.
Force Production
*
ΔV.mg protein-1
0.6
0.4
0.2
0.0
EV
Nr2f6
EV Nr2f6
52
Nr2f6

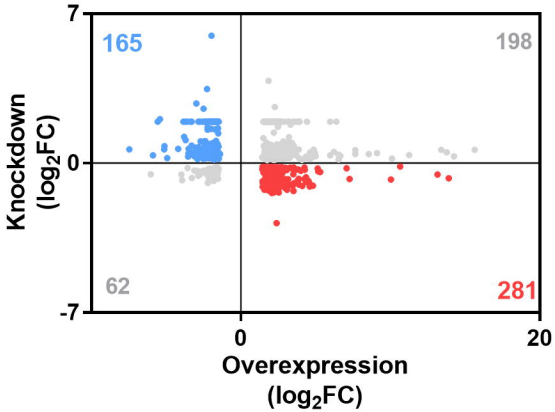
A
165
198
62
281
Knockdown (log2FC)
Overexpression (log2FC)
7
0
-7
0
20

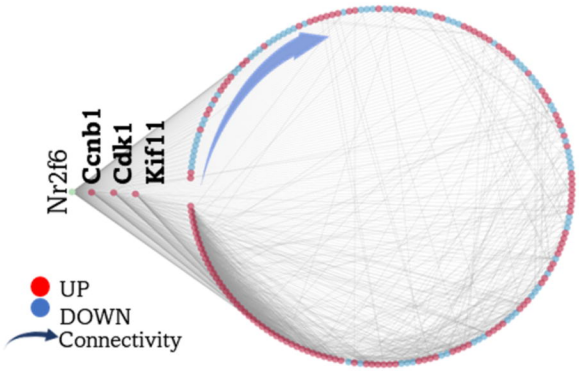
B
Nr2f6
Ccnb1
Cdk1
Kif11
UP
DOWN
Connectivity

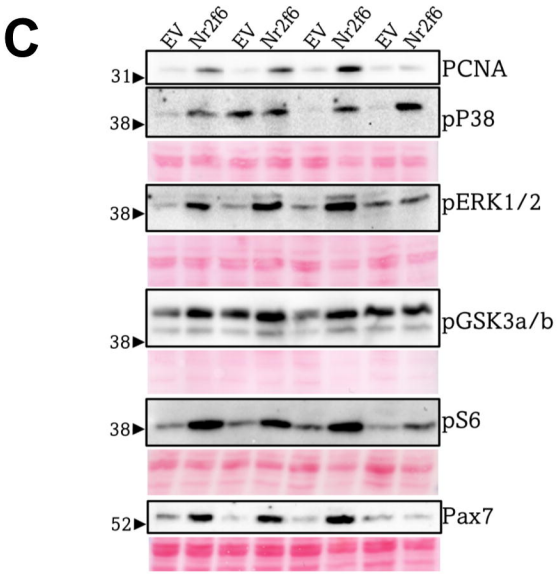
C
EV
Nr2f6
PCNA
pP38
pERK1/2
pGSK3a/b
pS6
Pax7
31
38
52

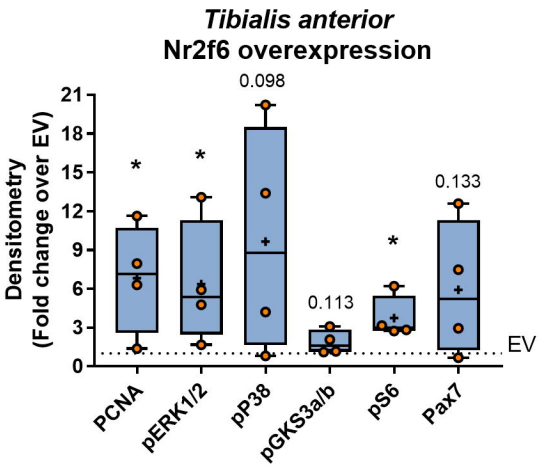
D
Tibialis anterior
Nr2f6 overexpression
Densitometry (Fold change over EV)
0.098
0.113
0.133
EV
PCNA
pERK1/2
pP38
pGKS3a/b
pS6
Pax7

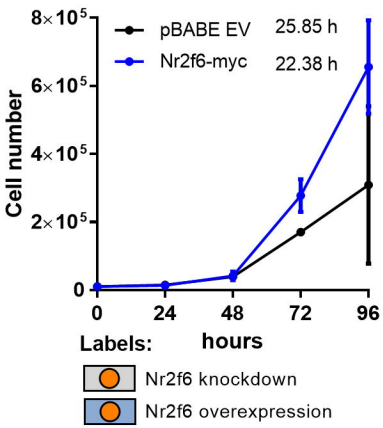
E
pBABE EV 25.85 h
Nr2f6-myc 22.38 h
Cell number
hours
Labels:
Nr2f6 knockdown
Nr2f6 overexpression

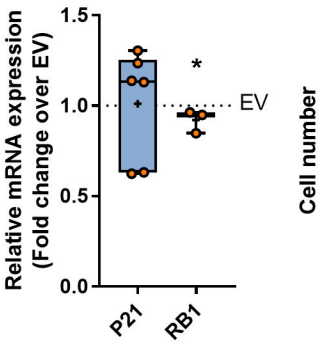
F
C2C12 Stable
Nr2f6 Overexpression
Relative mRNA expression (Fold change over EV)
EV
P21
RB1

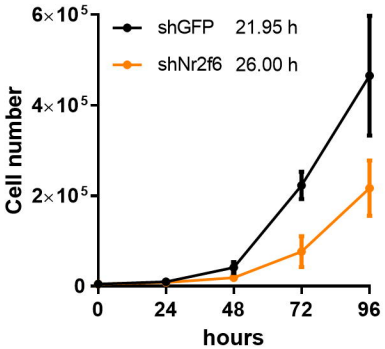
G
shGFP 21.95 h
shNr2f6 26.00 h
Cell number
hours

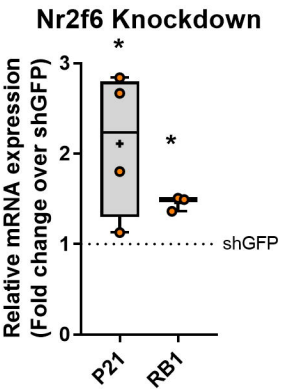
H
C2C12 Stable
Nr2f6 Knockdown
Relative mRNA expression (Fold change over shGFP)
shGFP
P21
RB1

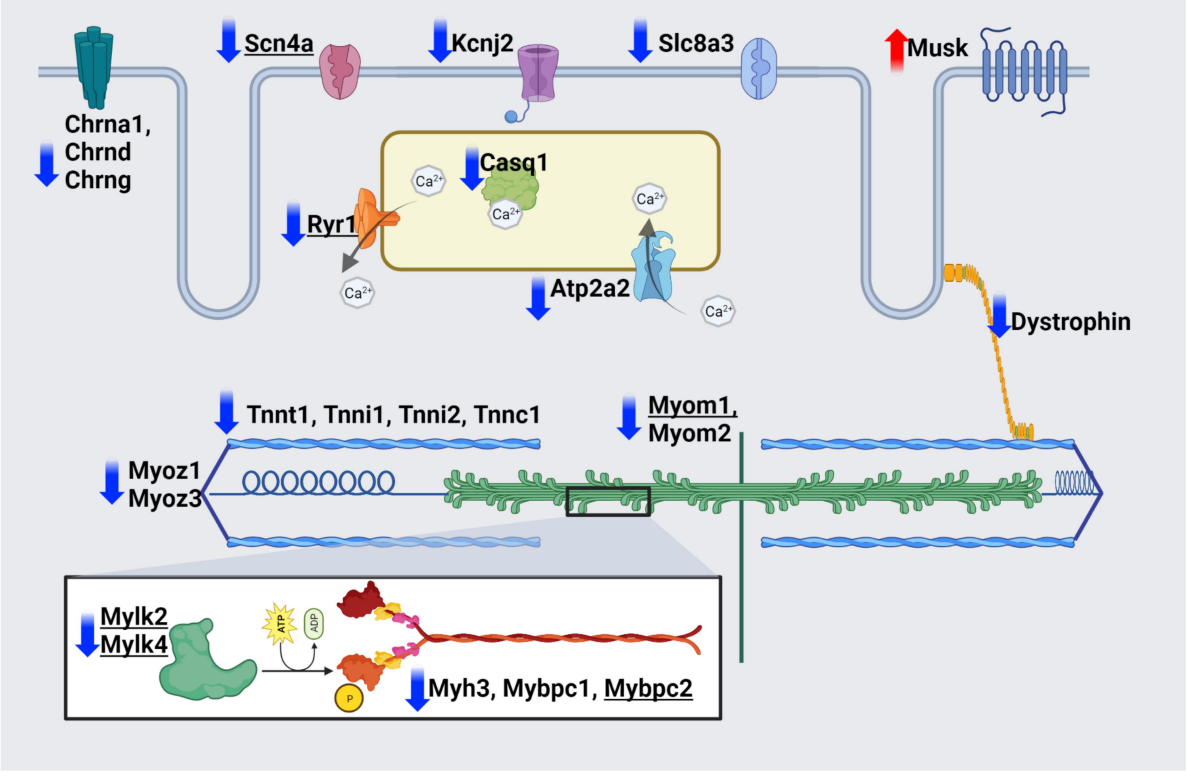
Scn4a
Kcnj2
Slc8a3
Musk
Chrna1,
Chrnd
Chrng
Casq1
Ryr1
Atp2a2
Ca2+
Dystrophin
Tnnt1, Tnni1, Tnni2, Tnnc1
Myom1,
Myom2
Myoz1
Myoz3
Mylk2
Mylk4
ATP
ADP
P
Myh3, Mybpc1, Mybpc2